2019

Single-grain OSL dating of fluvial terraces in the upper Hunter catchment, southeastern Australia

Xiao Fu
University of Wollongong, xiaofu@uow.edu.au

Tim J. Cohen
University of Wollongong, tcohen@uow.edu.au

Kirstie Fryirs
Macquarie University

Publication Details Citation

Fu, X., Cohen, T. J., & Fryirs, K. (2019). Single-grain OSL dating of fluvial terraces in the upper Hunter catchment, southeastern Australia. Faculty of Science, Medicine and Health - Papers: Part B. Retrieved from https://ro.uow.edu.au/smhpapers1/428

Single-grain OSL dating of fluvial terraces in the upper Hunter catchment, southeastern Australia

Abstract

Fluvial terraces in the upper Hunter catchment, southeastern Australia provide a long-term record of river activity in response to climate change in the late Quaternary. Single-grain optically stimulated luminescence (OSL) dating of quartz was applied in this study to investigate the timing of the formation of three fluvial terraces in the upper Hunter catchment. A detailed examination of luminescence properties of individual quartz grains revealed some correlation between their OSL decay rates, intrinsic brightness and dose saturation characteristics. Some quartz grains containing a higher proportion of non-fast components exhibit low brightness in OSL signals and high dose saturation levels. Some grains with slow OSL decays pass the standard rejection criteria, but are likely to yield underestimated equivalent doses (Des) because of a higher contribution of non-fast components, which are shown to have low thermal stability. Different rejection criteria, including the fast ratio, the dose saturation level and the OSL sensitivity criteria, were tested on the single-grain Deresults. Application of a fast ratio rejection criterion is able to successfully identify thermally unstable grains. A new rejection criterion based on dose saturation property was also applied to improve the age of one sample with a large De. Our dating results identify multiple phases of river valley aggradation in the upper Hunter catchment since late Marine Isotope Stage (MIS) 6; at ∼ 138 ka, ∼90-94 ka, ∼65 ka, ∼26 ka and ∼18 ka. The aggradational episodes of the terraces in the upper Hunter catchment are correlated with glacial or stadial periods since MIS 6. These phases of valley-floor aggradation are inferred to be a function of increased sediment supply during the cold periods resulting from strong periglacial activities in the adjacent Australian highlands.

Publication Details

Fu, X., Cohen, T. J. & Fryirs, K. (2019). Single-grain OSL dating of fluvial terraces in the upper Hunter catchment, southeastern Australia. Quaternary Geochronology, 49 115-122.

Single-grain OSL dating of fluvial terraces in the upper Hunter catchment, southeastern Australia

Xiao Fu [a] *, Tim J Cohen [b, c], Kirstie Fryirs [d]

[a] Centre for Archaeological Science, School of Earth and Environmental Sciences, University of Wollongong, Wollongong, NSW, 2522, Australia

[b] GeoQuEST Research Centre, School of Earth and Environmental Sciences, University of Wollongong, Wollongong, NSW 2522, Australia

[c] ARC Centre of Excellence for Australian Biodiversity and Heritage, University of Wollongong, Wollongong, NSW 2522, Australia

[d] Department of Environmental Sciences, Macquarie University, North Ryde, NSW 2109, Australia

Corresponding author: xiaofu@uow.edu.au; xiaofuled@gmail.com

Abstract: Fluvial terraces in the upper Hunter catchment, southeastern Australia provide a long-term record of river activity in response to climate change in the late Quaternary. Single-grain optically stimulated luminescence (OSL) dating of quartz was applied in this study to investigate the timing of the formation of three fluvial terraces in the upper Hunter catchment. A detailed examination of luminescence properties of individual quartz grains revealed some correlation between their OSL decay rates, intrinsic brightness and dose saturation characteristics. Some quartz grains containing a higher proportion of non-fast components exhibited low brightness in OSL signals and high dose saturation levels. Some grains with slow OSL decays passed the standard rejection criteria, but are likely to yield underestimated equivalent doses (D_es) because of a higher contribution of non-fast components, which were shown to have low thermal stability. Different rejection criteria, including the fast ratio, the dose saturation level and the OSL sensitivity criteria, were tested on the single-grain D_e results. The application of a fast ratio rejection criterion was able to successfully identify thermally unstable grains. A new rejection criterion based on dose saturation property was also applied to improve the age of one sample with a large D_e. Our dating results identify multiple phases of river valley aggradation in the upper Hunter catchment since late Marine Isotope Stage (MIS) 6; at ~ 138 ka, ~ 90-94 ka, ~ 65 ka, ~ 26 ka and ~ 18 ka. The aggradational episodes of the terraces are correlated with glacial or stadial periods since MIS 6 and these phases of valley-floor aggradation are inferred to be a function of increased sediment supply during the cold periods resulting from strong periglacial activities in the adjacent Australian highlands.

Keywords: Fluvial terrace, southeastern Australia, single-grain OSL, single-grain rejection criteria, glacial episode, LGM

1. Introduction

Fluvial sediments in Australia have provided important archives for assessing late Quaternary flow regime changes (e.g. Nanson et al., 1992). In southeastern Australia, abundant evidence exists of enhanced runoff conditions (relative to today) throughout the last full glacial cycle. A number of previous studies in this region have focused on large inland rivers draining west from the Great Dividing Range (GDR) which provides a record of river activity since Marine Isotope Stage (MIS) 5 (e.g. Nanson et al., 1992; Page et al., 1996, 2009; Kemp and Rhodes, 2010; Kemp et al., 2017). However, for the coastal draining catchments to the east of the GDR, the available fluvial record is less constrained and possibly shorter given the narrow valleys and resulting poorer preservation potential. In eastern New South Wales (NSW), the hydrological setting is characterised by a series of smaller coastal-draining catchments (< 1000 km^2) surrounded by much larger basins, such as the Hunter and Shoalhaven catchments which extend to the west of the great escarpment and with drainage areas > 5000 km^2 (Fig.1a). Previous studies have focused on small coastal valleys which mainly record post-Last Glacial Maximum (LGM) and Holocene valley-floor accumulation (e.g. Fryirs and Brierley, 1998; Brooks et al., 2003; Cohen and Nanson, 2008). Fewer studies (Nott et al., 2002; Nanson et al., 2003) have investigated the much larger catchments containing drainage areas above the escarpment (on the tablelands), despite preserving antecedent fluvial landforms of much greater antiquity (e.g. Nott et al., 2002). The reliable determination of ages of such terraces is important for exploring the reconstruction of long-term flow-regime changes east of the GDR and forms the basis for understanding the regional palaeoclimatic variations of southeastern Australia.

This paper presents a detailed single-grain optically stimulated luminescence (OSL) dating study for three fluvial terraces preserved in the upper Hunter catchment, the third largest coastal draining catchment in NSW. We report the characteristics of the OSL signals of individual quartz grains for the upper Hunter samples, as well as the sensitivity of their equivalent dose (D_e) estimates to different newly proposed single-grain rejection criteria (e.g. Duller, 2012). The new terrace chronologies are compared with climate cycles and existing fluvial records in the study region, and the implications for river responses to palaeoclimate changes are discussed.

2. Study sites and samples

The Hunter catchment is located on the central coast of NSW with an area of 22,000 km² (Figs.1a and b). It is one of the largest catchments in coastal NSW and extends west of the great escarpment in eastern Australia. This larger catchment, and specifically the upper Hunter, is located very near the headwaters of the Macquarie River, a major sub-catchment of the Murray-Darling Basin (MDB). Therefore the larger Hunter catchment shares morphological and climatic characteristics of the smaller coastal catchments but is also well situated to headwater rivers of the MDB from which the long record of flow-regime changes exist.

The upper Hunter catchment is located in the northeastern region of the basin (Fig.1b) and most of the rivers in the catchment are classified as confined or partly-confined. In these settings, lateral movement of the contemporary river courses are confined by bedrock valley margins or antecedent landforms formed under former flow regimes, such as fluvial terraces and alluvial fans (Fryirs and Brierley, 2010). These antecedent landforms not only provide confinement for modern river behaviour, but also record a long history of fluvial activity.

In this study we sampled three fluvial terrace sections in the upper Hunter catchment. Two fluvial terrace exposures, named the Razorback upper terrace and lower terrace, are located near the Razorback Bridge in the central east of catchment (Fig.1b). The terraces are ~ 600 m away from each other and are 10 to 13 m above the modern river channel (Figs.2b and d) and are located on the convex margin of the meander bends or at the channel inflection point. The Razorback upper terrace (UH-URB) is mainly composed of massive silty clay, overlying a thin unit of channel gravels with no bedrock exposed at the base of exposure (Fig. 2a). One OSL sample was collected from the lower part of this section. Three stratigraphic units were identified from the Razorback lower terrace (UH-LRB), including a bedrock strath at the base, overlain by a coarse gravel to cobble channel facies, underlying a silty clay channel-fill unit (Fig.2c). One sample UH-LRB was collected from the silty clay unit immediately above the gravel dominated channel facies.

The third sampled fluvial terrace section is on Kingdon Ponds at Wingen (Fig.1b), a tributary in the central west of the basin. This terrace (named the Kingdon Ponds terrace) is 10 m above the current channel bed (~5 m above the floodplain) (Fig.2 f) and is characterized by a complex stratigraphy of gravels and finer-grained facies (Fig.2e). The basal unit is a gravel lag (Unit A) underlying a cemented silty-clay unit at the bottom of the section (Unit B). Above the silty-clay unit is a complex stratigraphy of gravel-dominated facies comprising channel fill, trough-cross beds, matrix-supported massive and horizontally bedded units. These units reflect various phases of bar development and cut-and fill (Units C1-D3) that are terminated by debris flow deposits (Units E1-

E2). Atop the debris flow unit is a vertically accreted floodplain surface (Units F1-F3) but with coarse-grained lenses. Five samples KPW-1 to KPW-5 were collected from Units F1 to B from top to the bottom.

3. Methods

Single-grain quartz OSL dating was performed for all samples. OSL samples were prepared using the same method as detailed in Fu et al. (2017). Sand-sized (180-212 μm or 212-250 μm in diameter) quartz grains were separated and then etched for 40 minutes using 45% HF acid. OSL was measured on a Risø DA-20 TL/OSL reader. The OSL signals of individual grains were obtained by stimulation using a focused 10 mW green (532 nm) laser at 125°C for 1.8 s, and collected using an EMI9235QA photomultiplier tube through 7.5 mm Hoya U-340 filter. A single-aliquot regenerative dose (SAR) protocol (Murray and Wintle, 2000) was used to determine the D_es of individual grains, which includes an IR depletion-ratio test (Duller, 2003) applied to each grain at the end of the SAR sequence (using an infrared exposure of 100 s at 50°C) to detect any potential feldspar contamination. Based on dose recovery tests, the preheat temperatures for samples from the Razorback terraces and Kingdon Ponds terrace were chosen to be 240°C and 220°C, respectively .

All luminescence data were processed using the **R** packages 'numOSL' (Peng and Li, 2017) and 'Luminescence' (Kreutzer et al., 2017). The net OSL signal was calculated from the first 0.2 s of the OSL decay minus a background estimated from the last 0.3 s. All dose response curves (DRCs) were fitted using a general-order kinetics (GOK) function (Guralnik et al., 2015), which has been shown to be flexible and robust for fitting DRCs with different forms (Peng and Li, 2017). We applied the standard rejection criteria (e.g. Jacobs et al., 2006, 2008) as the basic grain selection criteria (Table S3). Besides these, three additional rejection criteria, including the fast ratio (FR) (Durcan and Duller, 2011; Duller, 2012), the dose saturation level (e.g. Thomsen et al., 2016) and the OSL sensitivity, were also tested on our samples, given that a broad dependence of natural D_e and overdispersion (OD) on these factors was observed for all of our samples (Section 4).

Environmental dose rates for all samples were derived from their U, Th and K contents measured using ICP-MS and ICP-OES techniques. Detailed dose rate information for all samples are summarised in Tables S1 and S2.

4. Results and discussion

4.1. Luminescence characteristics

For each of the samples, the quartz grains exhibited significant grain-to-grain variability in terms of OSL decay rate, inherent brightness and the shape of DRC. For grains that passed the standard rejection criteria, ~ 20-30% of grains showed OSL signals decaying to < 10% of the initial intensity after 0.2 s stimulation, suggesting the dominance of a fast component; nevertheless, there are also similar proportion of grains exhibited a remnant OSL > 30% of their initial intensities after 0.2 s stimulation, indicating a relatively high proportion of slower components in their OSL (e.g. Fig.S1a). In order to characterise the OSL decay rates for all samples, we calculated the FR of each grain for each sample, using the OSL signals of the natural test doses (T_n) and with the same integrals as proposed by Jacobs et al. (2013) (0-0.02 s for fast component, 0.18-0.22 s for medium and slow components). The median FR for the grains which passed the standard rejection criteria ranged from 4 to 7 for the seven samples. All samples show a broad distribution in FR (mostly range from ~1 to 40), suggesting that the proportion of the fast component varies considerably between grains for all of these samples (e.g. Fig.S1c).

The DRCs of the grains exhibit different shapes and considerable variation in dose saturation levels (e.g. Fig.S1b). When a single saturating exponential function was used to fit the DRCs of all grains, the obtained D_0 value ranged from ~ 30 to 300 Gy for grains from different samples, with a median D_0 value of ~ 120-130 Gy for each sample (e.g. Fig.S1d). Nevertheless, for each sample there are many of the grains whose DRCs are not well represented by a single exponential growth function, for which the D_0 values obtained using single saturating exponential fitting would have large inaccurate. To better compare the dose saturation properties of grains with variable forms of DRCs, we used the ratio between the sensitivity-corrected luminescence signals of two different regenerative doses to characterise the dose saturation characteristics of individual grains (also see Li et al., 2016). We name this ratio as the signal growth ratio (SGR), and in this study define it as the ratio between the fitted L_x/T_x values for two arbitrarily chosen regeneration doses of 200 and 50 Gy, derived from the DRC of each grain fitted using the GOK model (i.e. the higher the SGR is, the later the grain is getting saturated). Similar to the apparent D_0, the SGR varies significantly between grains for all samples, corresponding to their very different dose saturation levels (e.g. Fig.S1e).

Cumulative OSL brightness curves (Fig.S2) reveal significant variation in inherent brightness between grains with about 10% of the measured grains yielding ~ 90% of the total OSL signals. The intensity of T_n of the accepted grains (after standard rejection criteria) varies by 4-6 orders of magnitude (e.g. Fig.S1a). The sensitivity of sedimentary quartz grains has been suggested to be associated with multiple factors such as the source origin of the mineral grains and their sedimentary/thermal history (e.g. Li and Wintle, 1992; Pietsch et al., 2008; Sawakuchi et al., 2011; Fitzsimmons, 2011). These factors may also affect other luminescence properties of quartz grains including the relative proportion of the fast component and dose saturation properties, as suggested in previous studies (e.g. Chen et al., 2001; Lai et al., 2008; Gong et al., 2014, 2015). To explore the potential correlation between these luminescence properties, the FRs of quartz grains were compared against their T_n signals and SGRs for all sample (e.g. Fig.S3). We observed a moderate positive correlation between FR and T_n ($\rho = 0.5$) and a moderate negative correlation between FR and SGR ($\rho = -0.4$). This suggests that in general the grains with higher contribution from the fast component would be brighter and saturate earlier, and vice versa.

The positive correlation between FR and T_n is consistent with previous investigations which suggest that the sensitization of the quartz OSL signal (either by repeated dosing/bleaching, heating or inherited from source rock) is mainly related to the fast component (e.g. Preusser et al., 2009; Jeong and Choi, 2012); thus, grains with higher content of the fast component are expected to have a greater sensitivity. Gong et al. (2014, 2015) also observed that for their samples from Chinese deserts the quartz grains with higher content of non-fast components saturate later. This was attributed to the fact that the DRCs of medium and slow components saturate later than that of the fast component (Bailey, 2000b; Singarayer and Bailey, 2003; Rhodes et al., 2006). To check whether this is true for our samples, we examined the variation of SGR as a function of OSL measurement time for the quartz grains (the SGR(t) plot, similar to the D_e (t) plot of Bailey, 2000a). Fig.S4 shows examples of two grains with high (> 20) and low (< 2) FR. For both grains, the SGR shows an obvious increasing tendency towards the later integrals, suggesting that the non-fast components saturate later compared to the fast component. This observation also holds true for other grains from our samples. We therefore interpret that the negative correlation between SGR and FR is due to a greater contribution of the non-fast components to the bulk OSL signals of the slowly-decaying grains.

4.2. Dose recovery test

Single-grain dose recovery tests were carried out on samples UH-URB, KPW-2 and KPW-5 to validate the SAR protocol (Fig.S5). The dose recovery ratios (calculated using the central age model (CAM, Galbraith et al., 1999)) for the three samples are 0.97 ± 0.02, 0.99 ± 0.01 and 0.92 ± 0.02, after application of the standard rejection criteria. These results demonstrate that with our measurement conditions and the standard rejection criteria, we are able to recover a known laboratory dose accurately when the given doses are close to the natural D_es of our samples, except for the oldest sample KPW-5 (which were given a large surrogate natural dose of 234 Gy in the dose recovery test) whose dose recovery ratio was slightly less than unity. Changing preheat and cutheat conditions did not improve the results for KPW-5.

Sample KPW-5 has a high palaeodose and contains a lot of statured or near-saturated grains. It has been suggested that (e.g. Li et al., 2016; Thomsen et al., 2016) for this kind of sample, the measured D_e distribution can be truncated since some early-saturating grains may only be able to record D_es with lower values, and this can lead to underestimation in the dose recovery ratio and D_e estimate. Several studies suggested that removing early-saturating grains can improve the dose recovery ratios and D_e estimates for these samples (Gliganic et al., 2012; Demuro et al., 2015; Thomsen et al., 2016; Guo et al., 2017; Guérin et al., 2017). To test this, we applied a SGR rejection criterion in addition to the standard rejection criteria to the dose recovery dataset of KPW-5, i.e. accept grains only when their SGR values are larger than a threshold. Fig.S5f shows the dose recovery ratio of KPW-5 as a function of the SGR threshold. The dose recovery ratio increases gradually with the chosen SGR above which grains are rejected, while a plateau consistent with unity (at 1σ) has been reached when the SGR threshold is 2.1 or larger. These results suggest that rejecting early-saturating grains can help better recover the given dose for this specific sample. For other younger samples, application of the SGR selection makes no change in the dose recovery ratio (e.g. Fig.S5e). Fig.S6 shows the distribution of measured-to-given dose ratios for grains from UH-URB, KPW-2 (both applied standard rejection criteria) and KPW-5 (applied standard plus SGR rejection criteria). The OD values for the dose recovery results of the three samples are 8%, 7% and 15%, respectively.

Since in the natural D_e analysis we also tested another two rejection criteria—FR and T_n (see below), these two criteria were also tested on the dose recovery results. Figs.S5a-d show the dose recovery ratio as a function of the FR and T_n thresholds for samples UH-URB and KPW-5. For both samples, we observed no dependence of the dose recovery ratio on FR or the intensity of T_n. The results for the latter sample differ from Duller (2012), who observed that application of the FR rejection criterion can improve the dose recovery ratio at higher doses.

4.3. Natural D_e distribution and palaeodose estimation

Application of the standard rejection criteria to all samples resulted in 86-97% grains being rejected for D_e estimation (Table S3). The criteria that eliminate most grains are associated with the weak inherent brightness (T_n is within 3σ of the BG or relative standard error of T_n > 20%, rejected 71-

93% grains), while other criteria generally rejected less than 15% grains in total. After application of the standard rejection criteria, five out of the seven samples (UH-URB, UH-LRB, KPW-2, -4 and -5) showed medium OD values ranging from 28% to 46%, while other two samples (KPW-1 and -3) yielded high OD values of 144% and 92%, respectively.

The OD of the natural D_e dataset is associated with both intrinsic (e.g. luminescence properties (Galbraith et al., 2005)) and extrinsic factors (e.g. microdosimety, partial bleaching, post-depositional mixing). Duller (2012) initially suggested that applying a FR rejection criterion to single-grain datasets can reduce the intrinsic OD by rejecting grains with aberrant behaviours, whereas the efficacy of the FR rejection criterion on natural D_e and its OD has since been shown to be sample dependent (Jacobs et al., 2013; Fu et al., 2015; Feathers, 2015; Trauerstein et al., 2017). To test the rejection based on FR criteria for our samples, we applied different FR rejection threshold to our single-grain datasets. For the five samples with medium OD (see an example in Fig.3a), the CAM D_e increases with FR threshold until plateauing at a FR threshold of 4-5; meanwhile, the OD value also decreased to a plateau at about the same FR threshold. This is similar to the natural D_e data of Fu et al. (2015) and Feathers (2015), which showed that the quartz grains with low FR are likely to yield underestimated D_es, resulting in final D_e underestimation and OD increase. In contrast to Duller (2012) and Feathers (2015), we observed no dependence of the dose recovery ratio on FR (Fig.S6). We therefore deduce that the dependence of natural D_e on FR is unrelated to the performance of the grains in the SAR protocol, rather it is likely to be related to the thermal stability of the non-fast components, which have been shown to be unstable for dating (e.g. Li and Li, 2006; Steffen et al., 2008). To confirm this, we examined the D_e (t) plots and pulse annealing curves of quartz grains with low and high FR. The results show that the non-fast components in our samples yield underestimated D_e compared to the fast component, and grains with lower FR are thermally more unstable than those with higher FR (see details in Figs. S7 and S8). For the two samples with high OD, the dependence of D_e and OD on FR is weak. We infer that this is because the D_e dispersion of these two samples mainly arises from extrinsic factors (bioturbation, see below). Nevertheless, including grains with potential thermal stability problems may still obscure the real D_e distribution pattern for these samples.

Since a positive correlation between FR and intrinsic sensitivity has been observed (Fig.S3a), a T_n rejection criterion is also expected to discard unwanted grains which yield underestimated D_es. Fig.3b shows the D_e and OD of UH-URB as a function of the T_n threshold. As expected, plateaus in D_e and OD are achieved for brighter grains; the plateaus are consistent with those for the FR rejection threshold test (Fig.3a). But in general, application of the T_n rejection criterion has rejected more grains compared with FR rejection criterion without achieving any refined precision, and there lacks a uniform inter-sample standard for applying the sensitivity rejection criterion. Thus, we prefer the FR rejection criterion to the T_n rejection criterion in this paper.

On the basis of the above arguments, we used the FR as an additional rejection criterion for all of our samples, using a FR threshold value of 5 based on the D_e plateaus for our samples. This FR criterion has rejected ~ 1% to 9% of the grains for different samples in addition to the standard rejection criteria. Given that a dependence of the dose recovery ratio on the dose saturation property is observed for sample KPW-5 (Fig.S5f), we've also tested using the SGR as a rejection criterion for our samples, using grains which passed the standard rejection criteria and with FR > 5. We found the use of the SGR rejection criterion did not change the results for the six younger samples, suggesting that the single-grain ages of these samples are negligibly affected by dose saturation; but for the oldest sample KPW 5, the use of a SGR threshold criterion appears to be helpful in removing the bias in the single-grain D_e selection, as indicated by an increase in D_e with increasing SGR threshold and the achievement of a D_e plateau when the SGR threshold is tighten to a value of ~ 2.0 or higher (Fig. 4). This plateau range is also consistent with that of the dose recovery test for this sample (Fig.S5f). Based on this, we applied a SGR rejection criterion (using a threshold value of 2.1 according to the dose recovery test) in addition to the standard plus FR rejection criteria for sample KPW-5. Application of the SGR threshold criterion has further rejected ~ 2% of the grains for KPW-5.

The SGR threshold criterion has also been tested on all of the grains that passed the standard rejection criteria (i.e. without conducting the FR selection). By doing this, we've identified some grains in our samples which exhibit high dose saturation levels (high SGR) and low D_e values (Fig.S9a). A detailed examination of luminescence properties of these grains reveal that these grains are likely to contain more non-fast components, therefore can yield underestimated D_es due to low thermal stability; application of a FR rejection criterion can reject these grains for D_e estimation (see details in Figs.S9b-d).

Fig. 5 shows the final D_e distributions of all samples as radial plots. After application of the additional rejection criteria (FR or FR & SGR), the OD values for the five mediumly dispersed samples (UH-URB, UH-LRB, KPW-2, -4 and -5) were all reduced (from 28-46 % to 23-34%). The OD of these five samples are within the reported values for well-bleached samples (Arnold and Roberts, 2009); and the symmetrical single-grain D_e distributions of them indicate that they are sufficiently bleached. We have therefore applied a CAM to estimate the palaeodoses for these five samples. Samples KPW-1 and KPW-3 present high OD values even after application of the FR rejection criterion (161% and 89%, respectively). These two samples show strong mixing features in their D_e distributions, as evidenced by discrete D_e components being identified in the radial plots (Fig.5). We deduce that these two samples have experienced bioturbation after deposition, as we've observed plants growing on the outcrop and KPW-1 is also close to the terrace surface (Fig.2e). A finite mixture model (FMM) (Roberts et al., 2000) was therefore applied to these two samples for palaeodose evaluation (Table S4). A D_e population that comprised the majority (58%) of grains in the D_e distribution was identified for KPW-1, which possibly gives a good estimation for its burial dose. But for KPW-3, two major D_e populations with similar proportion were exhibited in the D_e dataset (42% and 38%, respectively), indicating the sample was severely mixed after deposition and ambiguity exists for identification of a D_e population related to deposition. We infer that the two grain populations may originate from two stratigraphic units representing two river aggradation events (i.e. grains from one unit were mixed into the other due to bioturbation), and we tentatively used the D_e values of the two major populations to give two potential depositional ages for this sample. These ages were treated with caution when doing the climate interpretation. Table S1 gives a summary of the palaeodoses and ages of all samples.

4.4. Chronologies of the terraces and their implications

The final ages for all of the samples were compared with glacial-interglacial cycles (Fig.6). The two samples collected from adjacent terraces of the upper Hunter River indicate two aggradational episodes of the river. Sample UH-LRB collected from the silty clay immediately above the coarse-gravel unit of the Razorback lower terrace yielded an age of 93.9 ± 5.7 ka, suggesting a floodplain accretion event occurred at mid-to-late MIS 5. Another sample UH-UHB collected from the silty clay deposits of the Razorback upper terrace yielded an age of 65.0 ± 4.1 ka, suggesting a later valley floor aggradation occurred in MIS 4. Further dating of the upper section of the two terraces will build more detailed age structures for these terraces.

The ages of the five samples collected from the Kingdon Ponds terrace are consistent with their stratigraphic order. The lowest sample from Unit B comprising of silty clay yielded an age of 137.7 ± 12.1 ka, suggesting an episode of floodplain accretion close to modern river level occurred in late MIS 6. The bottom of the coarse gravel unit (Unit C1; Fig.2) lying above Unit B was dated to be 90.5 ± 7.6 ka, suggesting a coarse-gravel bed river occupied this valley elevation at mid-to-late MIS 5, similar to the timing of the Razorback lower terrace in adjacent valley. A higher sample from Unit D1 returned two potential ages of 65.8 ± 10.8 ka and 26.6 ± 4.8 ka. The older age may represent a depositional event chronologically similar to the formation of the Razorback upper terrace. The younger age is indistinguishable with the age of the overlying debris deposits (Unit E1, dated to 25.7 ± 1.9 ka), atop which a silty clay unit (Unit F1) is aged at 18.3 ± 2.0 ka. These stratigraphic units with similar ages may reflect different phases of valley floor aggradation (including channel and floodplain deposition and alluvial fan deposition) occurred intermittently during MIS 2, albeit the age of Unit D1 (obtained from the severely mixed sample KPW-3) may need to be treated with caution.

Nott et al. (2002) and Nanson et al. (2003) have investigated large coastal draining rivers in NSW and extended the fluvial records of southeastern Australian coastal catchments to ~ 100 ka. Based on TL dating of fluvial sediments, these studies argued for an enhanced pluvial episode at (mid-to-late) MIS 5 and a declined fluvial activity at LGM. Broadly similar conclusions were achieved in earlier investigations on fluvial sediments in the Riverine Plain based on TL or OSL dating (e.g. Page et al., 1996; Kemp and Rhodes, 2010). Recently, a study on the Willandra Lakes on the Riverine Plain suggested these lakes were fed by the palaeo-sub branch of the Lachlan River (arising in the GDR) and maintained a high lake stand at the LGM (Kemp et al., 2017). Similar results by Mueller et al., (in press) have shown elevated discharge (relative to today) on the Murrumbidgee River at the LGM. In comparison, the fluvial terraces in the upper Hunter catchment also record fluvial aggradation in mid-to-late MIS 5 and the enhanced alluvial sedimentation in MIS 2, as recorded in the Kingdon Ponds terrace, which may be closely related to the LGM high lake level and river activity phase of the Riverine Plain.

The chronologies obtained in this study appear to suggest that all the river aggradation phases in the upper Hunter catchment occurred in glacial or stadial periods (MIS 6, MIS 5b, MIS 4 and MIS 2) (Fig.6). In Australia, fluvial sedimentation tends to be dominated by sediment availability (e.g. Nanson et al, 1992; Page and Nanson, 1996). A potential major source of sediment is the nearby ranges which have elevations of ~1000 - 1500m a.s.l. A recent study of Slee and Shulmeister (2015) has identified extensive periglacial landforms in eastern Australian mountain regions including the upper Hunter catchment. These periglacial landforms, whist undated, provide evidence for strong freeze-thaw processes throughout the late Quaternary and presumably have formed in the cold periods with adequate moisture. An increased sediment supply provided by the strong periglacial activities, together with increased runoff due to seasonal snowmelt (Reinfelds et al., 2014) and decreased sediment residence time due to variation of vegetation (Dosseto et al., 2010) during the cold episodes, is very likely to drive the aggradation of valley floors. If this hypothesis is true, there must be a regional similarity between the long-term fluvial records in areas affected by past periglacial processes. More chronological studies of other fluvial archives in large coastal draining catchments in southeastern Australia, such as the Shoalhaven River, should further test this hypothesis.

5. Conclusions

Chronologies of three fluvial terraces in the upper Hunter catchment in southeastern Australia were investigated using single-grain quartz OSL dating. Detailed luminescence investigations revealed some correlation between multiple luminescence properties of individual grains and their D_e values. Application of additional single-grain rejection criteria were found to reduce overdispersion arising from intrinsic factors and improve the dating results. Our dating results extended the fluvial record in southeastern Australia to MIS 6 and set a hypothesis that fluvial aggradation in the upper Hunter catchment is associated with glacial or stadial periods, which may be explained by enhanced sediment supply to the catchment resulting from strong periglacial activities during the cold episodes.

Acknowledgements

This study was supported by an Australia Research Council Discovery Project grant (DP110103081) to TC. XF thanks the ARC Laureate Fellowship grant (FL130100116) to Professor Richard Roberts for financial support for the LED 2017 conference. We also thank John Janson and Luke Gliganic for their support in the collection of the Upper Hunter at Razorback samples, Luke Gliganic for sample preparation of these samples and to Daniela Mueller for preparing some of the KPW samples. We also would like to thank Bo Li and Zenobia Jacobs for giving helpful comments on the early results of this study. This paper also benefitted by the comments of an anonymous reviewer.

References

Arnold, L.J., Roberts, R.G., 2009. Stochastic modelling of multi-grain equivalent dose (De) distributions: implications for OSL dating of sediment mixtures. Quaternary Geochronology 4, 204–230.

Bailey, R.M., 2000a. The interpretation of quartz optically stimulated luminescence equivalent dose versus time plots. Radiation Measurements 32, 129–140.

Bailey, R.M., 2000b. The slow component of quartz optically stimulated luminescence. Radiation Measurements 32, 233–246.

Brooks, A.P., Brierley, G.J., Millar, R.G., 2003. The long-term control of vegetation and woody debris on channel and flood-plain evolution: insights from a paired catchment study in southeastern Australia. Geomorphology 51, 7–29.

Chen, G., Murray, A.S., Li, S.-H., 2001. Effect of heating on the quartz dose-response curve. Radiation Measurements 33, 59–63.

Cohen, T.J., Nanson, G.C., 2008. Topographically associated but chronologically disjunct late Quaternary floodplains and terraces in a partly confined valley, south-eastern Australia. Earth Surface Processes and Landforms 33, 424–443.

Demuro, M., Arnold, L.J., Parés, J.M., Sala, R., 2015. Extended-range luminescence chronologies suggest potentially complex bone accumulation histories at the Early-to-Middle Pleistocene palaeontological site of Huéscar-1 (Guadix-Baza basin, Spain). Quaternary International 389, 191–212.

Dosseto, A., Hesse, P.P., Maher, K., Fryirs, K., Turner, S., 2010. Climatic and vegetation control on sediment dynamics during the last glacial cycle. Geology 38, 395–398.

Duller, G.A.T., 2012. Improving the accuracy and precision of equivalent doses determined using the optically stimulated luminescence signal from single grains of quartz. Radiation Measurements 47, 770–777.

Duller, G.A.T., 2003. Distinguishing quartz and feldspar in single grain luminescence measurements. Radiation Measurements 37, 161–165.

Durcan, J.A., Duller, G.A.T., 2011. The fast ratio: A rapid measure for testing the dominance of the fast component in the initial OSL signal from quartz. Radiation Measurements 46, 1065–1072.

Feathers, J., 2015. Luminescence dating at Diepkloof Rock Shelter – new dates from single-grain quartz. Journal of Archaeological Science 63, 164–174.

Fitzsimmons, K., 2011. An assessment of the luminescence sensitivity of Australian quartz with respect to sediment history. Geochronometria 38, 199–208.

Fryirs, K., Brierley, G., 1998. The character and age structure of valley fills in upper Wolumla Creek catchment, south coast, New South Wales, Australia. Earth Surface Processes and Landforms 23, 271–287.

Fryirs, K., Brierley, G.J., 2010. Antecedent controls on river character and behaviour in partly confined valley settings: Upper Hunter catchment, NSW, Australia. Geomorphology 117, 106–120.

Fu, X., Cohen, T.J., Arnold, L.J., 2017. Extending the record of lacustrine phases beyond the last interglacial for Lake Eyre in central Australia using luminescence dating. Quaternary Science Reviews 162, 88–110.

Fu, X., Li, S.-H., Li, B., 2015. Optical dating of aeolian and fluvial sediments in north Tian Shan range, China: Luminescence characteristics and methodological aspects. Quaternary Geochronology 30, 161–167.

Galbraith, R.F., Roberts, R.G., Laslett, G.M., Yoshida, H., Olley, J.M., 1999. Optical Dating of Single and Multiple Grains of Quartz from Jinmium Rock Shelter, Northern Australia: Part I, Experimental Design and Statistical Models. Archaeometry 41, 339–364.

Galbraith, R.F., Roberts, R.G., Yoshida, H., 2005. Error variation in OSL palaeodose estimates from single aliquots of quartz: a factorial experiment. Radiation Measurements 39, 289–307.

Gliganic, L.A., Jacobs, Z., Roberts, R.G., 2012. Luminescence characteristics and dose distributions for quartz and feldspar grains from Mumba rockshelter, Tanzania. Archaeological and Anthropological Sciences 4, 115–135.

Gong, Z., Sun, J., Lü, T., 2015. Investigating the components of the optically stimulated luminescence signals of quartz grains from sand dunes in China. Quaternary Geochronology 29, 48–57.

Gong, Z., Sun, J., Lü, T., Tian, Z., 2014. Investigating the optically stimulated luminescence dose saturation behavior for quartz grains from dune sands in China. Quaternary Geochronology 22, 137–143.

Guérin, G., Frouin, M., Tuquoi, J., Thomsen, K.J., Goldberg, P., Aldeias, V., Lahaye, C., Mercier, N., Guibert, P., Jain, M., Sandgathe, D., McPherron, S.J.P., Turq, A., Dibble, H.L., 2017. The complementarity of luminescence dating methods illustrated on the Mousterian sequence of the Roc de Marsal: A series of reindeer-dominated, Quina Mousterian layers dated to MIS 3. Quaternary International 433, 102–115.

Guo, Y.-J., Li, B., Zhang, J.-F., Yuan, B.-Y., Xie, F., Roberts, R.G., 2017. New ages for the Upper Palaeolithic site of Xibaimaying in the Nihewan Basin, northern China: implications for small-tool and microblade industries in north-east Asia during Marine Isotope Stages 2 and 3. Journal of Quaternary Science 32, 540–552.

Guralnik, B., Li, B., Jain, M., Chen, R., Paris, R.B., Murray, A.S., Li, S.-H., Pagonis, V., Valla, P.G., Herman, F., 2015. Radiation-induced growth and isothermal decay of infrared-stimulated luminescence from feldspar. Radiation Measurements 81, 224–231.

Jacobs, Z., Duller, G.A.T., Wintle, A.G., 2006. Interpretation of single grain De distributions and calculation of De. Radiation Measurements 41, 264–277.

Jacobs, Z., Hayes, E.H., Roberts, R.G., Galbraith, R.F., Henshilwood, C.S., 2013. An improved OSL chronology for the Still Bay layers at Blombos Cave, South Africa: further tests of single-grain dating procedures and a re-evaluation of the timing of the Still Bay industry across southern Africa. Journal of Archaeological Science 40, 579–594.

Jacobs, Z., Roberts, R.G., Galbraith, R.F., Deacon, H.J., Grün, R., Mackay, A., Mitchell, P., Vogelsang, R., Wadley, L., 2008. Ages for the Middle Stone Age of Southern Africa: Implications for Human Behavior and Dispersal. Science 322, 733–735.

Jeong, G.Y., Choi, J., 2012. Variations in quartz OSL components with lithology, weathering and transportation. Radiation Measurements 10, 320–326.

Jouzel, J., Masson-Delmotte, V., Cattani, O., Dreyfus, G., Falourd, S., Hoffmann, G., Minster, B., Nouet, J., Barnola, J.M., Chappellaz, J., Fischer, H., Gallet, J.C., Johnsen, S., Leuenberger, M., Loulergue, L., Luethi, D., Oerter, H., Parrenin, F., Raisbeck, G., Raynaud, D., Schilt, A., Schwander, J., Selmo, E., Souchez, R., Spahni, R., Stauffer, B., Steffensen, J.P., Stenni, B., Stocker, T.F., Tison, J.L., Werner, M., Wolff, E.W., 2007. Orbital and Millennial Antarctic Climate Variability over the Past 800,000 Years. Science 317, 793–796.

Kemp, J., Pietsch, T., Gontz, A., Olley, J., 2017. Lacustrine-fluvial interactions in Australia's Riverine Plains. Quaternary Science Reviews 166, 352–362.

Kemp, J., Rhodes, E.J., 2010. Episodic fluvial activity of inland rivers in southeastern Australia: Palaeochannel systems and terraces of the Lachlan River. Quaternary Science Reviews 29, 732–752.

Kreutzer, S., Dietze, M., Burow, C., Fuchs, M. C., Schmidt, C., Fischer, M., Friedrich, J., 2017. Luminescence: Comprehensive Luminescence Dating Data Analysis. R package version 0.7.5. https://CRAN.R-project.org/package=Luminescence

Lai, Z., Brückner, H., Fülling, A., Zöller, L., 2008. Effects of thermal treatment on the growth curve shape for OSL of quartz extracted from Chinese loess. Radiation Measurements 43, 763–766.

Li, B., Jacobs, Z., Roberts, R.G., 2016. Investigation of the applicability of standardised growth curves for OSL dating of quartz from Haua Fteah cave, Libya. Quaternary Geochronology 35, 1–15.

Li, B., Li, S.-H., 2006. Comparison of De estimates using the fast component and the medium component of quartz OSL. Radiation Measurements 41, 125–136.

Li, S.-H., Wintle, A.G., 1992. Luminescence sensitivity change due to bleaching of sediments. Nuclear Tracks and Radiation Measurements 20, 567–573.

Mueller, D., Jacobs, Z., Cohen, T.J., Price, D.M., Reinfelds, I.V., Shulmeister, J. Revisiting an arid LGM using fluvial archives: A luminescence chronology for palaeochannels of the Murrumbidgee River, southeastern Australia. Journal of Quaternary Science, in press.

Murray, A.S., Wintle, A.G., 2000. Luminescence dating of quartz using an improved single-aliquot regenerative-dose protocol. Radiation Measurements 32, 57–73.

Nanson, G.C., Cohen, T.J., Doyle, C.J., Price, D.M., 2003. Alluvial evidence of major late-Quaternary climate and flow-regime changes on the coastal rivers of New South Wales, Australia. Palaeohydrology: Understanding Global Change. Gregory K, Benito G (eds). Wiley, Chichester, 233–258.

Nanson, G.C., Price, D.M., Short, S.A., 1992. Wetting and drying of Australia over the past 300 ka. Geology 20, 791–794.

Nott, J., Price, D., Nanson, G., 2002. Stream response to Quaternary climate change: evidence from the Shoalhaven River catchment, southeastern highlands, temperate Australia. Quaternary Science Reviews 21, 965–974.

Page, K., Nanson, G., Price, D., 1996. Chronology of Murrumbidgee River palaeochannels on the Riverine Plain, southeastern Australia. Journal of Quaternary Science 11, 311–326.

Page, K.J., Kemp, J., Nanson, G.C., 2009. Late Quaternary evolution of Riverine Plain paleochannels, southeastern Australia. Australian Journal of Earth Sciences 56, S19–S33.

Peng, J., Li, B., 2017 Single-aliquot regenerative-dose (SAR) and standardised growth curve (SGC) equivalent dose determination in a batch model using the R Package 'numOSL'. Ancient TL 35, 32-53.

Pietsch, T.J., Olley, J.M., Nanson, G.C., 2008. Fluvial transport as a natural luminescence sensitiser of quartz. Quaternary Geochronology 3, 365–376.

Preusser, F., Chithambo, M.L., Götte, T., Martini, M., Ramseyer, K., Sendezera, E.J., Susino, G.J., Wintle, A.G., 2009. Quartz as a natural luminescence dosimeter. Earth-Science Reviews 97, 184–214.

Reinfelds, I., Swanson, E., Cohen, T., Larsen, J., Nolan, A., 2014. Hydrospatial assessment of streamflow yields and effects of climate change: Snowy Mountains, Australia. Journal of Hydrology 512, 206–220.

Rhodes, E.J., Singarayer, J.S., Raynal, J.-P., Westaway, K.E., Sbihi-Alaoui, F.Z., 2006. New age estimates for the Palaeolithic assemblages and Pleistocene succession of Casablanca, Morocco. Quaternary Science Reviews 25, 2569–2585.

Roberts, R.G., Galbraith, R.F., Yoshida, H., Laslett, G.M., Olley, J.M., 2000. Distinguishing dose populations in sediment mixtures: a test of single-grain optical dating procedures using mixtures of laboratory-dosed quartz. Radiation Measurements 32, 459–465.

Sawakuchi, A.O., Guedes, C.C.F., DeWitt, R., Giannini, P.C.F., Blair, M.W., Nascimento, D.R., Faleiros, F.M., 2012. Quartz OSL sensitivity as a proxy for storm activity on the southern Brazilian coast during the Late Holocene. Quaternary Geochronology 13, 92–102.

Singarayer, J.S., Bailey, R.M., 2003. Further investigations of the quartz optically stimulated luminescence components using linear modulation. Radiation Measurements 37, 451–458.
Slee, A., Shulmeister, J., 2015. The distribution and climatic implications of periglacial landforms in eastern Australia. Journal of Quaternary Science 30, 848–858.
Steffen, D., Preusser, F., Schlunegger, F., 2009. OSL quartz age underestimation due to unstable signal components. Quaternary Geochronology 4, 353–362.
Thomsen, K.J., Murray, A.S., Buylaert, J.P., Jain, M., Hansen, J.H., Aubry, T., 2016. Testing single-grain quartz OSL methods using sediment samples with independent age control from the Bordes-Fitte rockshelter (Roches d'Abilly site, Central France). Quaternary Geochronology 31, 77–96.
Trauerstein, M., Lowick, S.E., Preusser, F., Veit, H., 2017. Testing the suitability of dim sedimentary quartz from northern Switzerland for OSL burial dose estimation. Geochronometria 44, 66–76.

Figure captions

Fig.1. (a) Map showing the coastal catchments of New South Wales, Australia and the location of the Hunter catchment. (b) Map of the Hunter catchment. The square indicates the location of the upper Hunter catchment. Stars indicate the locations of the sampling sites: UHR—Upper Hunter at Razorback; KPW—Kingdon Ponds at Wingen (Fryirs, unpublished data).

Fig.2. (a) Photograph showing the Razorback upper terrace exposure. (b) Transect of the Razorback upper terrace generated from the SRTM 30m digital elevation model (DEM). (c) Photograph showing the Razorback lower terrace exposure. (d) Transect of the Razorback lower terrace generated from the SRTM 30m DEM. (e) Photograph showing the Kingdon Ponds terrace exposure with unit boundaries (solid black line) and tentative unit or sub-unit boundaries (dashed line). Unit A is the basal gravels, Unit B is a fine-grained cemented facies, Units C1 to E2 are comprised of cobble and gravel units – mostly matrix-supported. Units F1-F3 includes thin gravel and sand lenses underlying fine-grained overbank material. (f) Valley cross-section showing the geomorphic setting of the Kingdon Ponds terrace (Fryirs, unpublished data). Elevations in (b), (d) and (f) are expressed as Australian Height Datum (AHD) elevation.

Fig.3. (a) CAM D_e (filled circles) and OD (open diamonds) of sample UH-URB against the fast ratio rejection threshold. (b) CAM D_e (filled circles) and OD (open diamonds) of sample UH-URB against the T_n rejection threshold.

Fig.4. CAM D_es (filled circles) and OD (open circles) of sample KPW-5 against the signal growth ratio rejection threshold, for grains that passed the standard rejection criteria and with fast ratio > 5.

Fig.5. Radial plots showing the single-grain D_e distributions of all samples. All datapoints are for grains which passed the standard rejection criteria. The closed circles and open triangles represent grains accepted and rejected by additional rejection criteria (FR > 5 & SGR > 2.1 for KPW-5 and FR > 5 for other samples), respectively. The shaded bands for samples UH-URB, UH-LRB, KPW-2, -4 and -5 are centred on their weighted mean D_es calculated using the CAM (for grains that passed the standard plus additional rejection criteria). The shaded bands for samples KPW-1 and -3 are centred on the weighted mean D_es for each grain population obtained using the FMM (for grains passed the standard plus additional rejection criteria).

Fig.6. Plot showing a comparison of the OSL ages with MIS stages and late Quaternary temperature anomaly recovered from Antarctic ice core (Jouzel et al., 2007). Grey bars represent glacial and stadial episodes. Diamonds represent ages of samples from the Razorback terraces. Circles represent ages of samples from Kingdon Ponds terrace. The open circles indicate two potential ages of the severely mixed sample KPW-3.

Figure 1

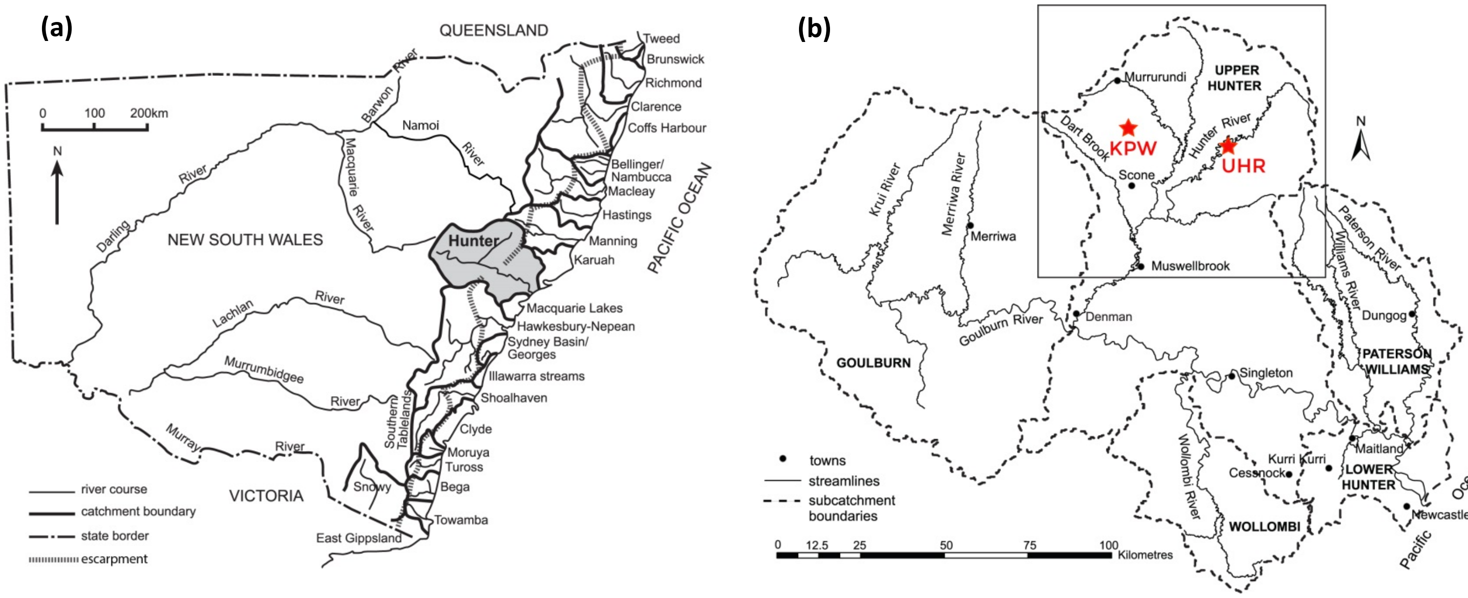
(a)
QUEENSLAND
Tweed
Brunswick
Richmond
Clarence
Coffs Harbour
Bellinger/
Nambucca
Macleay
Hastings
Manning
Karuah
PACIFIC OCEAN
0 100 200km
N
Barwon River
Namoi
River
Macquarie
River
Darling
River
NEW SOUTH WALES
Hunter
Macquarie Lakes
Hawkesbury-Nepean
Sydney Basin/
Georges
Illawarra streams
Shoalhaven
Lachlan
River
Murrumbidgee
River
Southern
Tablelands
Clyde
Moruya
Tuross
Bega
Towamba
Murray
River
VICTORIA
Snowy
East Gippsland
river course
catchment boundary
state border
escarpment
(b)
Murrurundi
UPPER
HUNTER
N
Dart Brook
KPW
Hunter River
UHR
Scone
Krui River
Merriwa River
Merriwa
Muswellbrook
Paterson River
Williams River
Dungog
Goulburn River
Denman
GOULBURN
PATERSON
WILLIAMS
Singleton
Wollombi River
Maitland
Kurri Kurri
Cessnock
LOWER
HUNTER
WOLLOMBI
Newcastle
Pacific
Ocean
towns
streamlines
subcatchment
boundaries
0 12.5 25 50 75 100 Kilometres

Figure 2

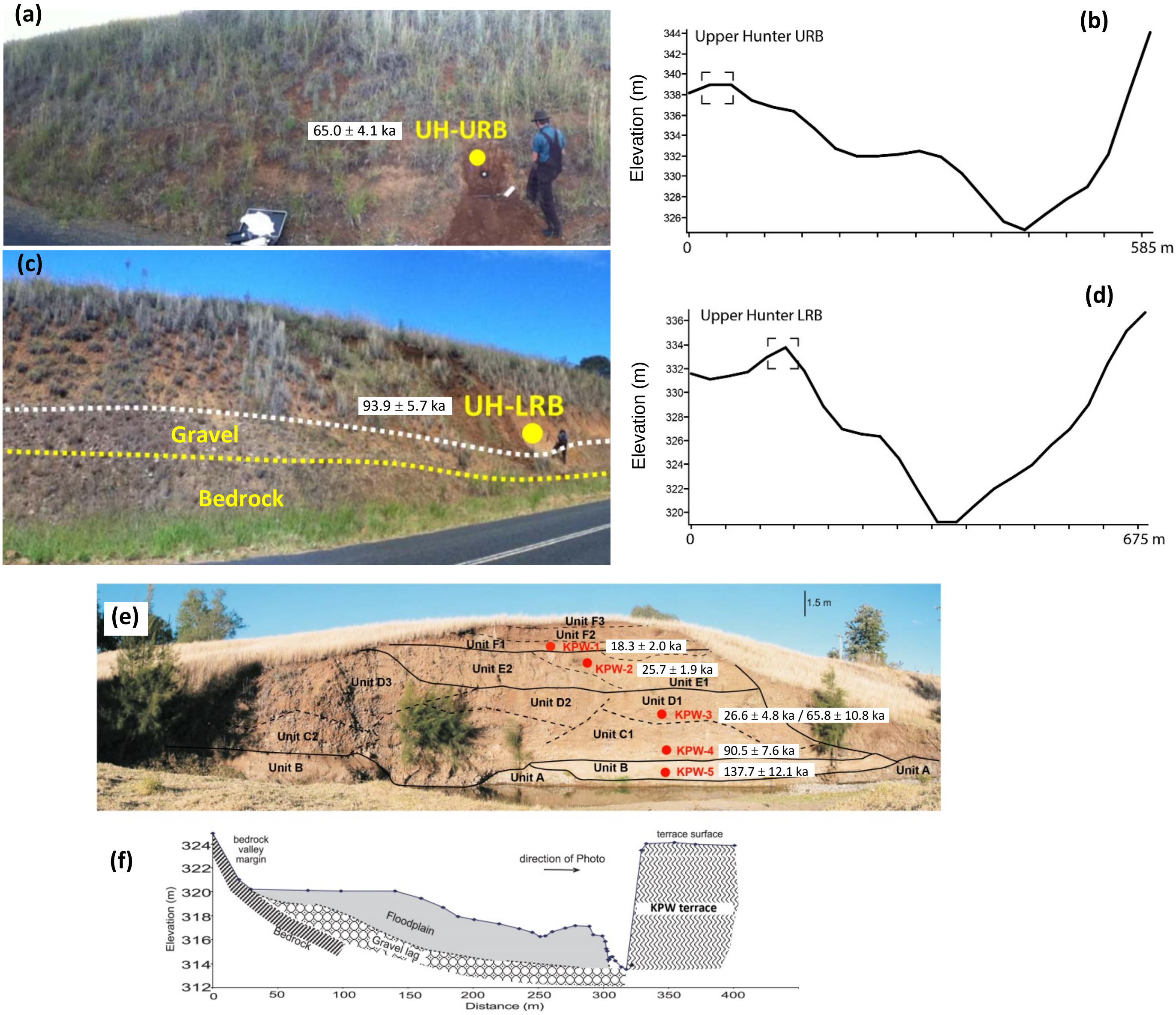
(a)
65.0 ± 4.1 ka
UH-URB
(b)
Upper Hunter URB
Elevation (m)
344
342
340
338
336
334
332
330
328
326
0
585 m
(c)
93.9 ± 5.7 ka
UH-LRB
Gravel
Bedrock
(d)
Upper Hunter LRB
Elevation (m)
336
334
332
330
328
326
324
322
320
0
675 m
(e)
1.5 m
Unit F3
Unit F2
Unit F1
KPW-1
18.3 ± 2.0 ka
KPW-2
25.7 ± 1.9 ka
Unit E2
Unit E1
Unit D3
Unit D2
Unit D1
KPW-3
26.6 ± 4.8 ka / 65.8 ± 10.8 ka
Unit C2
Unit C1
KPW-4
90.5 ± 7.6 ka
Unit B
Unit B
KPW-5
137.7 ± 12.1 ka
Unit A
Unit A
(f)
bedrock valley margin
direction of Photo
terrace surface
KPW terrace
Floodplain
Bedrock
Gravel lag
Elevation (m)
324
322
320
318
316
314
312
0
50
100
150
200
250
300
350
400
Distance (m)

Figure 3

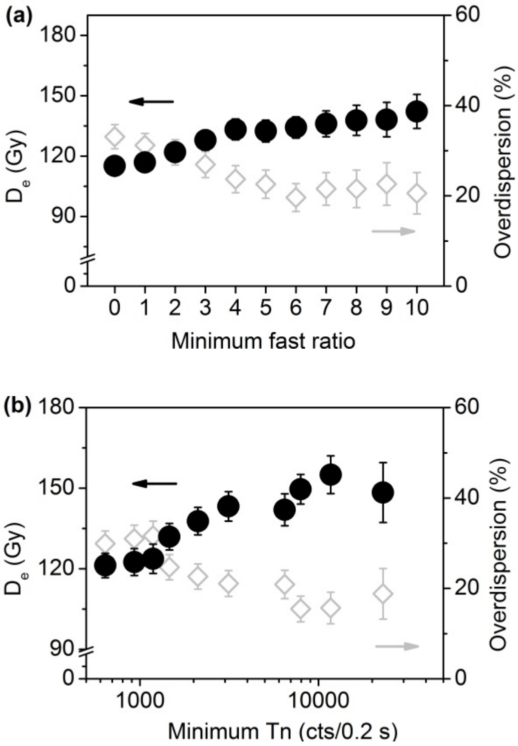
(a)
De (Gy)
Overdispersion (%)
Minimum fast ratio
(b)
De (Gy)
Overdispersion (%)
Minimum Tn (cts/0.2 s)

Figure 4

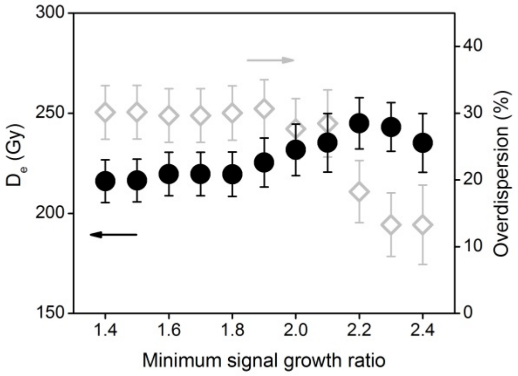

300
250
200
150
40
30
20
10
0
1.4
1.6
1.8
2.0
2.2
2.4
D_e (Gy)
Overdispersion (%)
Minimum signal growth ratio

Figure 5

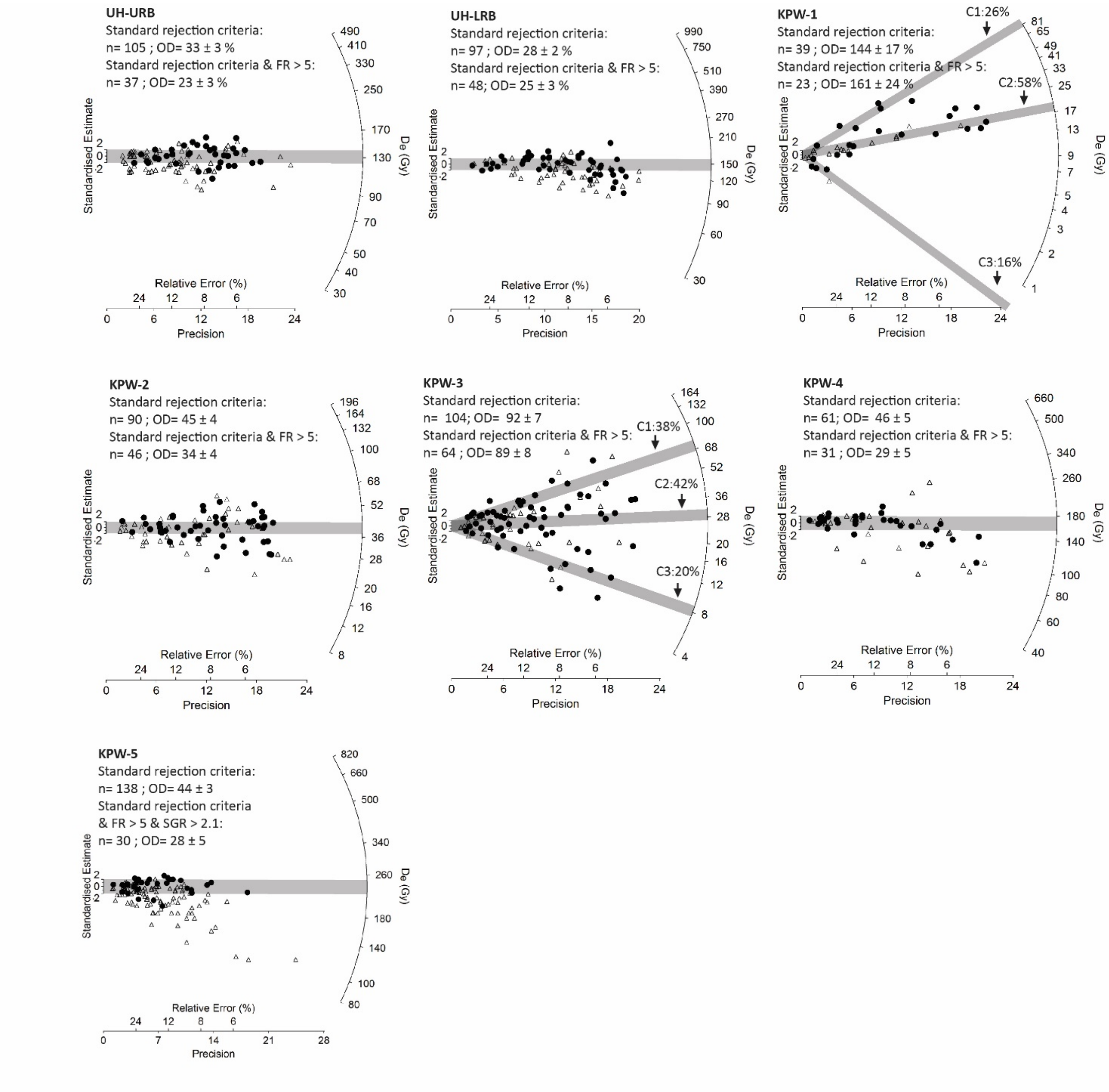
UH-URB
Standard rejection criteria:
n= 105 ; OD= 33 ± 3 %
Standard rejection criteria & FR > 5:
n= 37 ; OD= 23 ± 3 %
UH-LRB
Standard rejection criteria:
n= 97 ; OD= 28 ± 2 %
Standard rejection criteria & FR > 5:
n= 48; OD= 25 ± 3 %
KPW-1
Standard rejection criteria:
n= 39 ; OD= 144 ± 17 %
Standard rejection criteria & FR > 5:
n= 23 ; OD= 161 ± 24 %
C1:26%
C2:58%
C3:16%
KPW-2
Standard rejection criteria:
n= 90 ; OD= 45 ± 4
Standard rejection criteria & FR > 5:
n= 46 ; OD= 34 ± 4
KPW-3
Standard rejection criteria:
n= 104; OD= 92 ± 7
Standard rejection criteria & FR > 5:
n= 64 ; OD= 89 ± 8
C1:38%
C2:42%
C3:20%
KPW-4
Standard rejection criteria:
n= 61; OD= 46 ± 5
Standard rejection criteria & FR > 5:
n= 31 ; OD= 29 ± 5
KPW-5
Standard rejection criteria:
n= 138 ; OD= 44 ± 3
Standard rejection criteria
& FR > 5 & SGR > 2.1:
n= 30 ; OD= 28 ± 5
Standardised Estimate
Relative Error (%)
Precision
De (Gy)

604 **Figure 6**

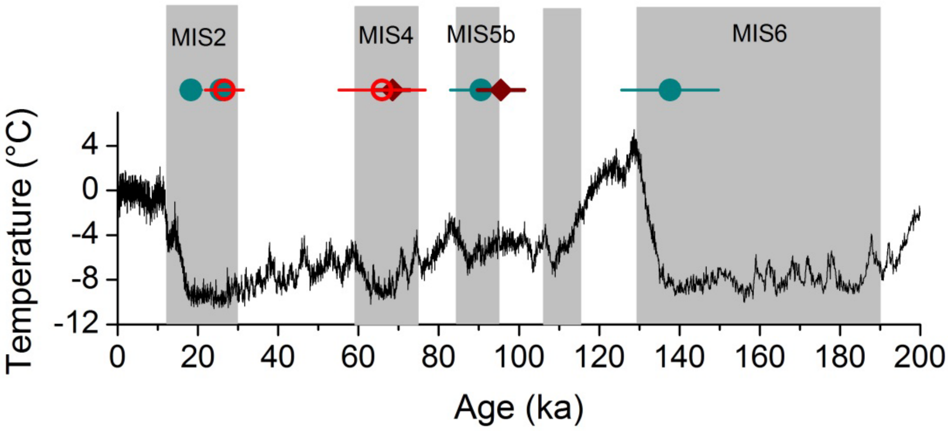
MIS2
MIS4
MIS5b
MIS6
Temperature (°C)
4
0
-4
-8
-12
0
20
40
60
80
100
120
140
160
180
200
Age (ka)

Single-grain OSL dating of fluvial terraces in the upper Hunter catchment, southeastern Australia

-Supplementary Information-

Xiao Fu [a] *, Tim J Cohen [b, c], Kirstie Fryirs [d]

[a] Centre for Archaeological Science, School of Earth and Environmental Sciences, University of Wollongong, Wollongong, NSW, 2522, Australia

[b] GeoQuEST Research Centre, School of Earth and Environmental Sciences, University of Wollongong, Wollongong, NSW 2522, Australia

[c] ARC Centre of Excellence for Australian Biodiversity and Heritage, University of Wollongong, Wollongong, NSW 2522, Australia

[d] Department of Environmental Sciences, Macquarie University, North Ryde, NSW 2109, Australia

Corresponding author: xiaofu@uow.edu.au ; xiaofuled@gmail.com

Table S1 Summary of dose rate information, equivalent doses (D_es) and ages

Sample	Site	Depth (m)	Grain size (μm)	Moisture content (%) [a]	Dose rate (Gy/ka) [b]			Total dose rate (Gy/ka) [c]	Accepted/ measured grains [d]	OD (%)	Age model	D_e (Gy) [e]	Age (ka)
					Beta	Gamma	Cosmic						
UH-URB	Upper Hunter @Razorback upper terrace	4.5	180-212	5	1.18 ± 0.06	0.66 ± 0.02	0.16 ± 0.02	2.04 ± 0.09	37/1000	23 ± 3	CAM	132.44 ± 5.40	65.0 ± 4.1
UH-LRB	Upper Hunter @Razorback lower terrace	6.5	180-212	5	0.87 ± 0.04	0.54 ± 0.02	0.14 ± 0.01	1.58 ± 0.07	48/1000	25 ± 3	CAM	148.23 ± 5.77	93.9 ± 5.7
KPW-1	Kingdon Ponds @Wingen	1.55	212-250	10	0.54 ± 0.03	0.26 ± 0.01	0.18 ± 0.02	1.00 ± 0.05	23/1300	161 ± 24	FMM	18.32 ± 1.70	18.3 ± 2.0
KPW-2	Kingdon Ponds @Wingen	2.05	180-212	10	0.87 ± 0.05	0.50 ± 0.02	0.17 ± 0.02	1.57 ± 0.08	46/800	34 ± 4	CAM	40.31 ± 2.13	25.7 ± 1.9
KPW-3	Kingdon Ponds @Wingen	6.6	212-250	10	0.62 ± 0.03	0.31 ± 0.07	0.13 ± 0.01	1.09 ± 0.05	64/900	89 ± 8	FMM (C1)	71.90 ± 11.29	65.8 ± 10.8
											FMM (C2)	29.02 ± 5.01	26.6 ± 4.8
KPW-4	Kingdon Ponds @Wingen	8	180-212	7	1.11 ± 0.05	0.59 ± 0.04	0.12 ± 0.01	1.86 ± 0.10	31/600	29 ± 5	CAM	168.11 ± 10.34	90.5 ± 7.6
KPW-5	Kingdon Ponds @Wingen	9	180-212	20	0.96 ± 0.05	0.61 ± 0.02	0.10 ± 0.01	1.71 ± 0.10	30/1200	28 ± 5	CAM	235.25 ± 14.62	137.7 ± 12.1

[a] Based on measured field moisture contents. The relative uncertainty for moisture content was assigned to 25%.

[b] Beta and gamma dose rates were derived from ICP-MS/OES analysis. The measured U, Th and K concentrations were converted into beta and gamma dose rates using conversion factors of Guérin et al. (2011), and corrected for the attenuations of grain size (Guérin et al., 2012) and moisture content (Nathan and Mauz, 2008). Cosmic dose rate was estimated following Prescott and Hutton (1994), taking into account of the geomagnetic latitude, altitude and burial depth of the samples. For sample KPW-4 which has a heterogeneous gamma dose rate within 30 cm, the model of Aitken et al. (1985, p. 289-293) has been applied to correct for the layer to layer difference in gamma dose rate.

[c] The total dose rates include an internal dose rate of 0.03 ± 0.01 Gy/ka, estimated using U and Th contents reported by Bowler et al. (2003).

[d] The accepted grains are grains passing the standard rejection criteria plus the additional rejection criteria (FR > 5 & SGR > 2.1 for KPW-5 and FR > 5 for other samples).

[e] For the two mixed samples KPW-1 and KPW-3, the D_e values were derived from the major grain populations fitted using FMM (Table S4). It is noted that for KPW-3 there are two main grain populations with similar proportion (Table S4). We calculated two potential ages for this sample based on these two populations.

Table S2 Summary of U, Th and K concentrations measured using ICP-MS/OES

Sample [a]	**U (ppm)**	**Th (ppm)**	**K (%)**
UH-URB	1.17 ± 0.06	4.80 ± 0.24	1.35 ± 0.07
UH-LRB	1.01 ± 0.05	4.57 ± 0.23	0.94 ± 0.05
KPW-1	0.33 ± 0.02	1.39 ± 0.07	0.72 ± 0.04
KPW-2	0.81 ± 0.04	3.99 ± 0.20	1.06 ± 0.05
KPW-3	0.40 ± 0.02	1.90 ± 0.07	0.81 ± 0.02
KPW-4-UG	0.67 ± 0.03	3.77 ± 0.15	0.96 ± 0.04
KPW-4	0.97 ± 0.04	6.57 ± 0.26	1.26 ± 0.05
KPW-4-LG	0.66 ± 0.03	3.41 ± 0.14	1.05 ± 0.04
KPW-5	1.10 ± 0.04	6.44 ± 0.26	1.23 ± 0.05

[a] Sample KPW-4 was collected from a 10 cm thick sand lens within a stratigraphic unit mainly comprising coarse gravels. Samples KPW-4-UG and KPW-4-LG were collected from coarse gravel layers above and below the sand lens, which were used for correcting for gamma dose heterogeneity for sample KPW-4.

Table S3 Summary of the single-grain OSL rejection details

Sample	**UH-URB**	**UH-LRB**	**KPW-1**	**KPW-2**	**KPW-3**	**KPW-4**	**KPW-5**
Total measured grains	1000	1000	1300	800	900	600	1200
Reason for rejecting grains from D_e analysis	%	%	%	%	%	%	%
Tn < 3σ background	58	65	84	68	66	62	60
RSE of Tn exceeds 20%	20	13	9	12	13	14	12
Recycling ratio ≠ 1 at ±2σ	2	1	1	1	2	1	2
OSL-IR depletion ratios <1 at ±2σ	5	1	1	2	1	2	1
Recuperation > 5%	1	1	0	0	1	0	0
Anomalous dose response / unable to perform DRC fit	3	7	2	6	4	8	5
Saturated grains	1	2	0	0	1	3	7
Zero dose grains	0	1	0	0	2	0	0
Fast ratio < 5	7	5	1	6	4	5	9
SGR > 2.1	N/A	N/A	N/A	N/A	N/A	N/A	2
Sum of rejected grains (%)	96	95	98	94	93	95	97
Sum of accepted grains (%)	4	5	2	6	7	5	3

Table S4 A summary of D_e value for each D_e component and the proportion of grains in each D_e component for samples fitted using the finite mixture model

Sample	**OD (%)**	**σ_b (%)[a]**	**k**	**D_e (Gy) [b]**	**Proportion (%)[b]**
				0.58 ± 0.20	16
KPW-1	161 ± 24	31	3	**18.32 ± 1.70**	**58**
				83.37 ± 12.51	26
				8.12 ± 1.28	20
KPW-3	89 ± 8	35	3	**29.02 ± 5.01**	**42**
				71.90 ± 11.29	**38**

[a] The optimal σ_b value used for fitting the finite mixture model was determined based on the maximum log likelihood (llik) and the Bayes Information Criterion (BIC) (Roberts et al., 2000).

[b] D_e components shown in bold are used for age estimation.

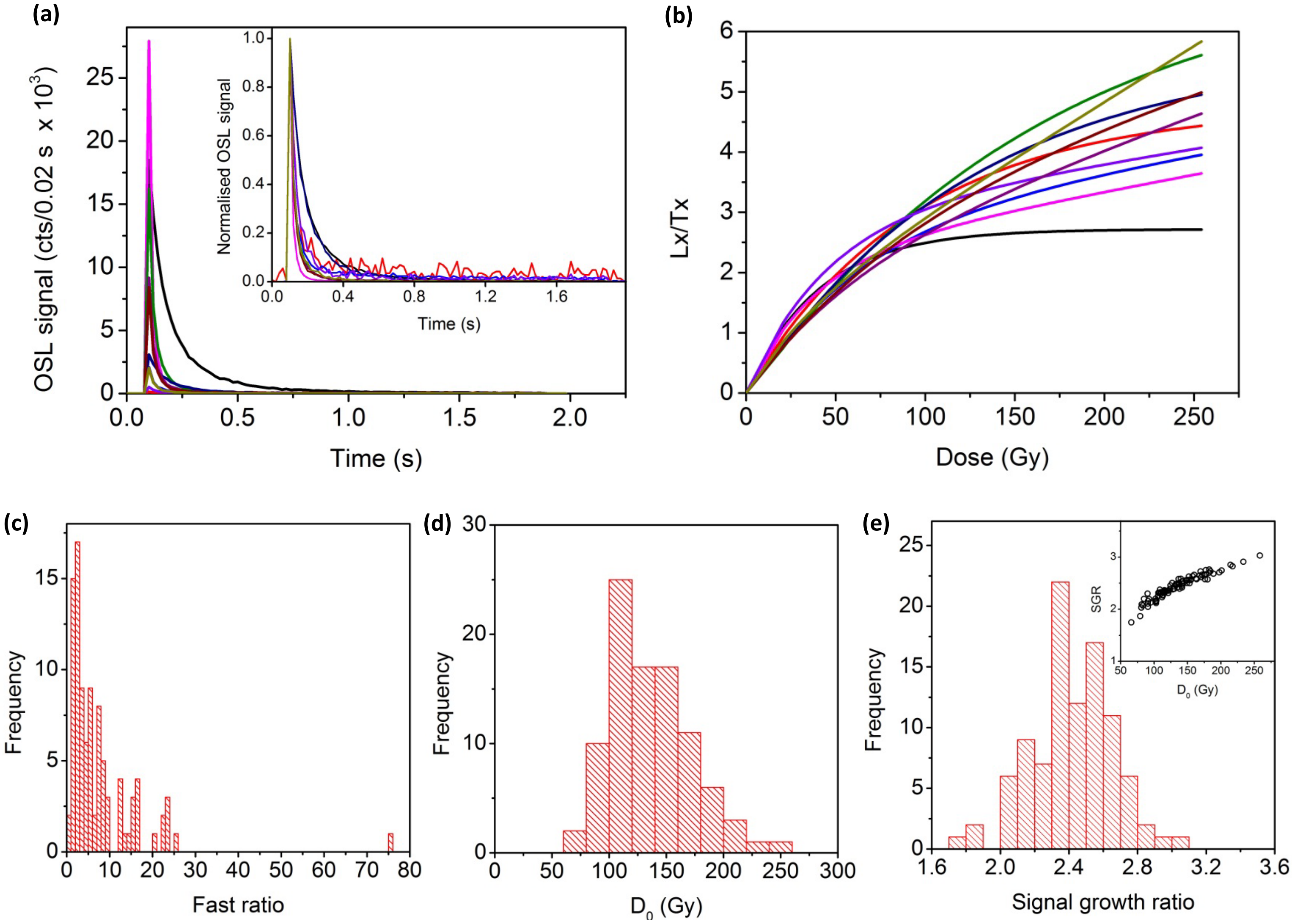

Fig.S1. (a) Single-grain OSL decay curves of 10 representative grains from sample UH-LRB, in response to a test dose of 23 Gy. The inset shows the same OSL decay curves which are normalised to the OSL counts of the first channel; (b) Single-grain OSL dose response curves of 10 representative grains from sample UH-LRB; (c) Fast ratio distribution of 97 grains from sample UH-LRB which pass the standard rejection criteria shown as histogram; (d) D_0 distribution of 93 (out of 97) grains from sample UH-LRB which pass the standard rejection criteria shown as histogram. The D_0 values were obtained by fitting the dose repose curve of each grain using a single saturating exponential function; (e) Signal growth ratio (SGR) of 97 grains from sample UH-LRB which pass the standard rejection criteria shown as histogram. The SGR is defined as the ratio between the fitted sensitivity-corrected OSL values for two regenerative doses—200 Gy and 50 Gy—obtained from the dose response curve of each grain fitted using a general-order kinetics (GOK) function (Guralnik et al., 2015). The inset shows the D_0 value against the SGR value for all grains.

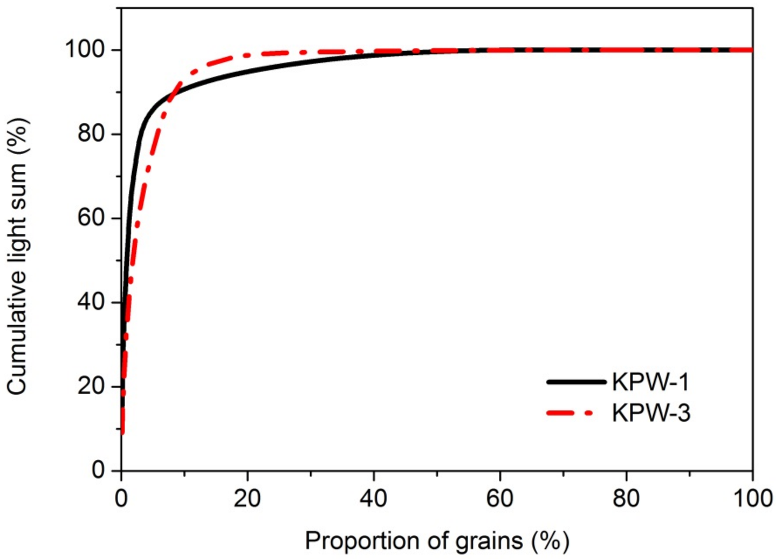

Fig.S2. Cumulative light sum plots for two representative samples KPW-1 and KPW-3.

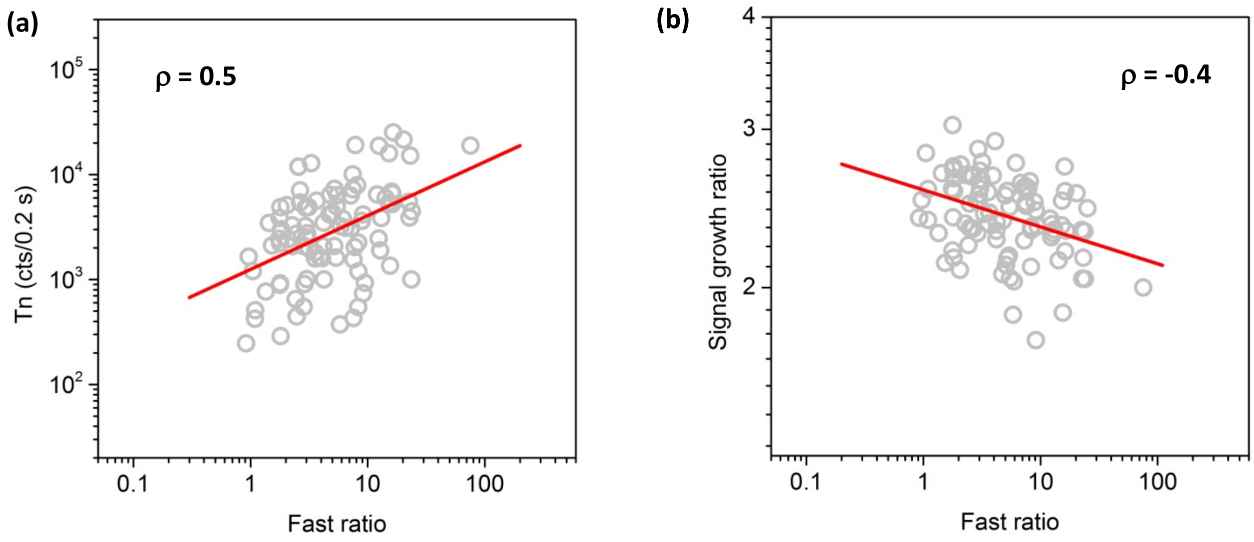

Fig.S3. (a) Fast ratio against Tn for 97 grains from sample UH-LRB which pass the standard rejection criteria; (b) Fast ratio against signal growth ratio for the same grains in (a). In both figures the red lines represent the best linear fit of the dataset. Both figures are in log-log scale.

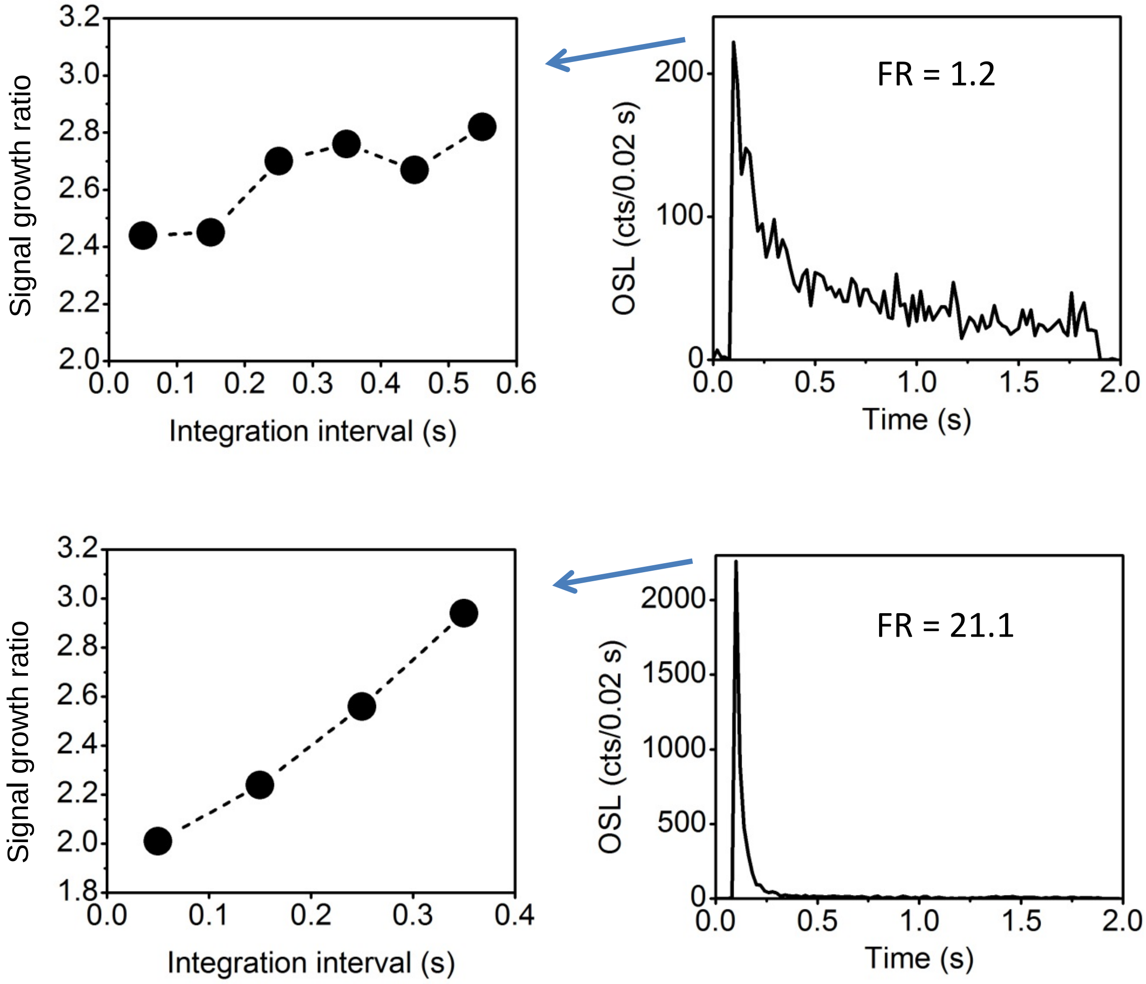

Fig.S4. Left panels: Signal growth ratio (SGR) plotted as a function of OSL measurement time (SGR (t) plot) for two grains from sample KPW-4 with different fast ratios (FRs). An increase in signal growth ratio towards the later integrals suggests that the non-fast components saturate later than the fast component; Right panels: OSL decay curves of the two grains in response to a test dose of 35 Gy.

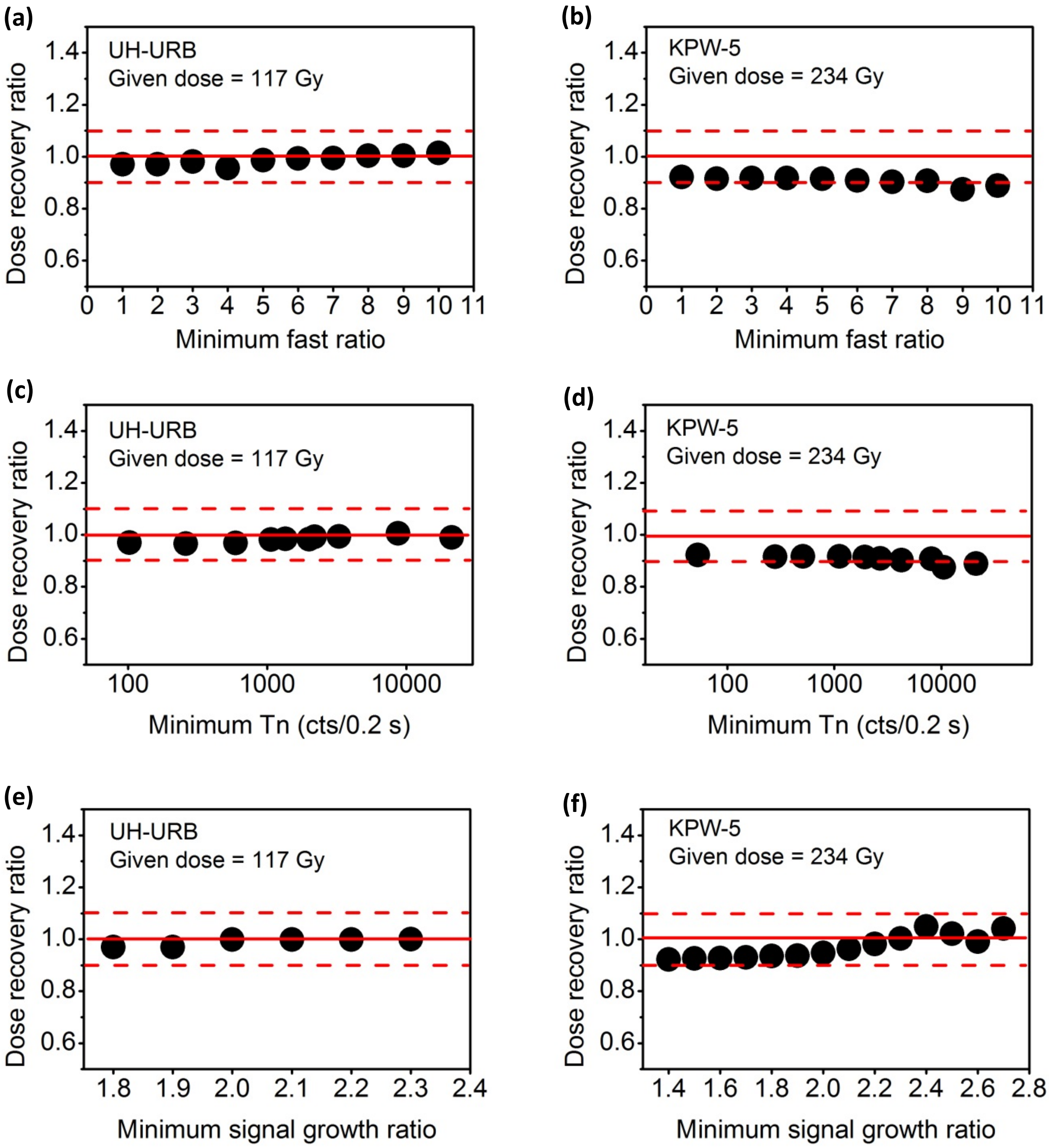

Fig.S5. Dose recovery ratio for samples UH-URB and KPW-5 shown as a function of (a) and (b): the fast ratio rejection threshold; (c) and (d): the Tn rejection threshold; and (e) and (f): the signal growth ratio rejection threshold.

(a)

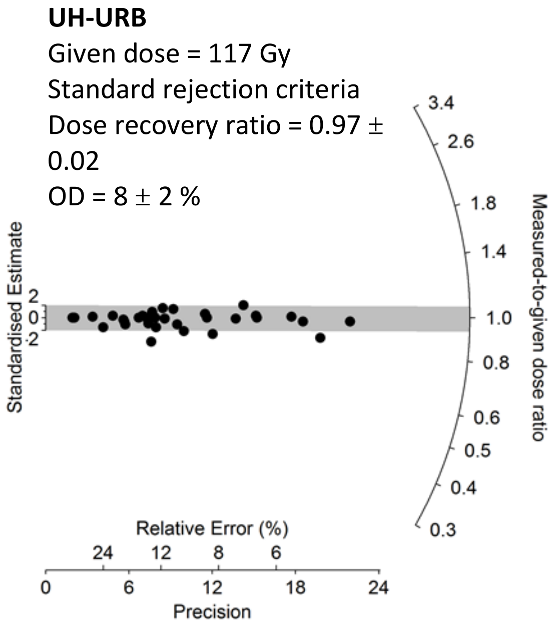

(b)

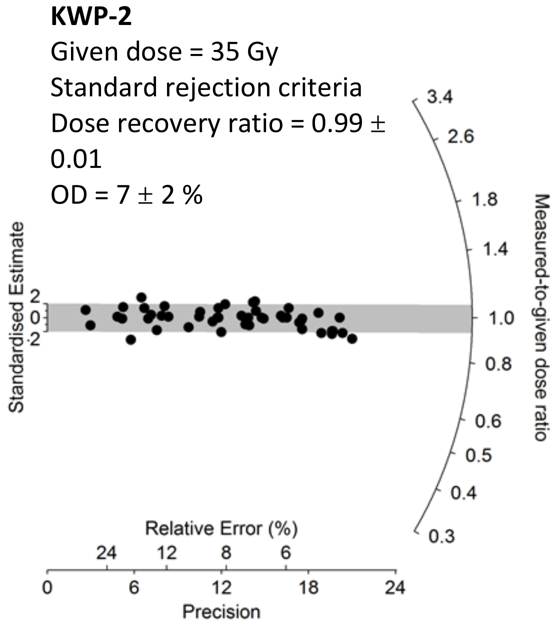

(c)

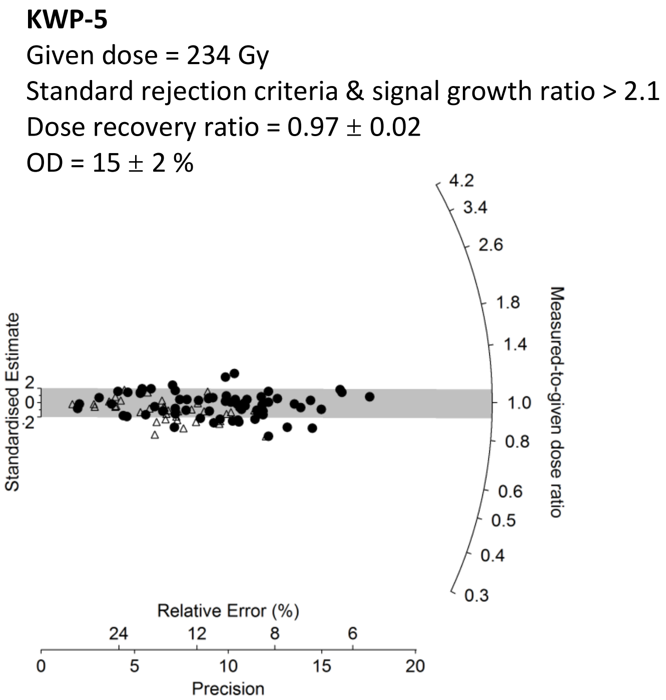

Fig.S6. Dose recovery test results for three representative samples UH-URB, KPW-2 and KPW-5 shown as radial plots. In the experiments, quartz grains of each sample were first bleached using a Dr Hönle UVACUBE 400 solar simulator for 1 hour to remove the natural signals, and then given a beta dose close to their natural D_es before measuring using the SAR protocol. For KPW-5, using all grains which pass the standard rejection criteria yields a slightly underestimated dose recovery ratio of 0.92 ± 0.02. After application of an additional signal growth ratio (SGR) rejection criterion using a SGR rejection threshold of 2.1, the dose recovery ratio is refined to 0.97 ± 0.02. The open triangles in Fig.S6c represent grains rejected by the signal growth ratio rejection criterion.

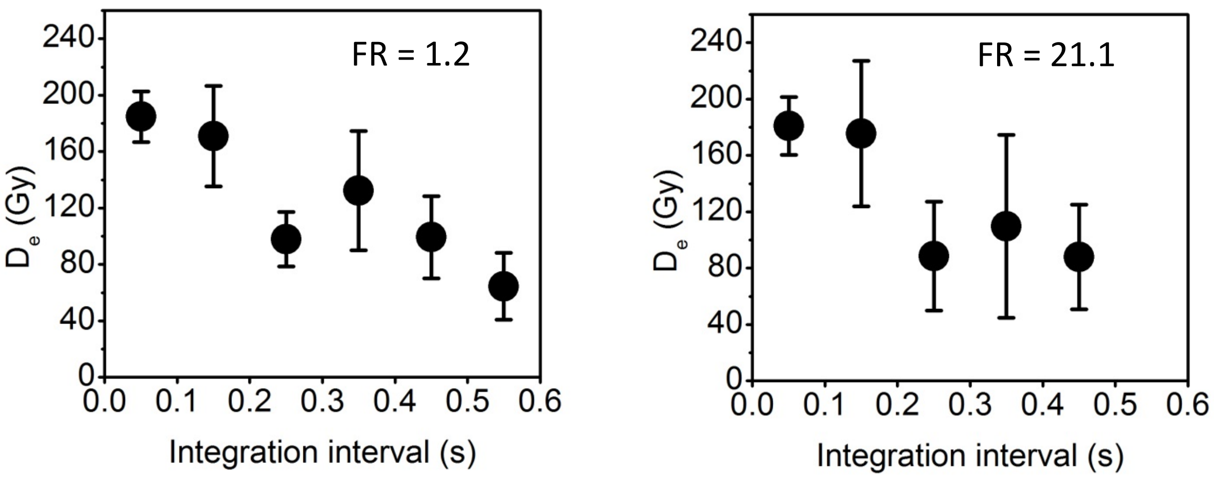

Fig.S7. D_e (t) plots (Bailey, 2000) of two grains from sample KPW-4 with different fast ratios (FRs) (the same grains as in Fig.S4). A decrease in D_e towards the later integrals was observed, which is often associated with unstable non-fast components (e.g. Li and Li, 2006; Steffen et al., 2009).

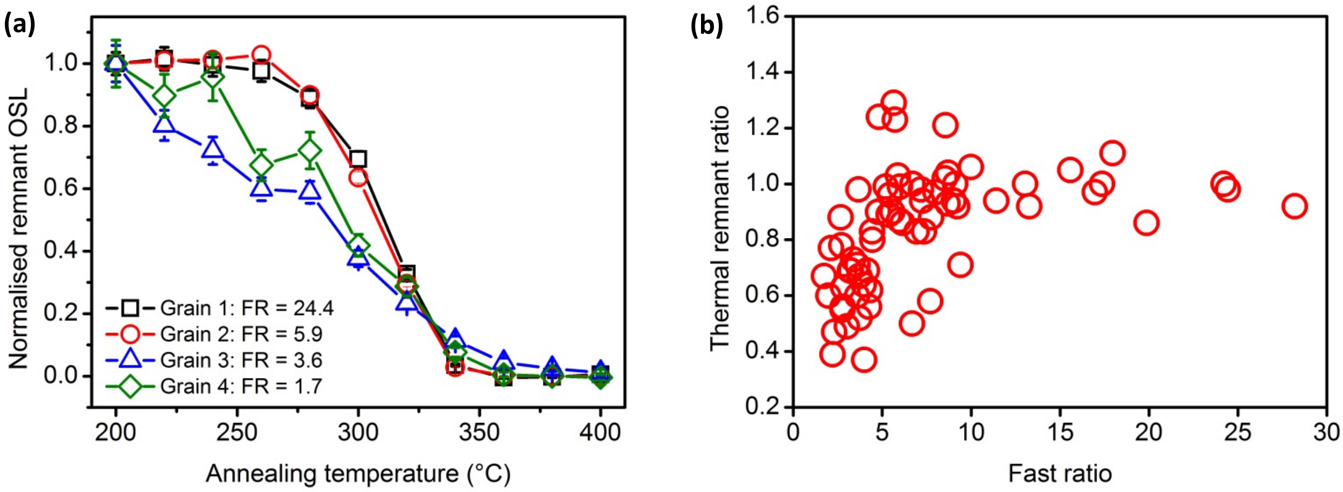

Fig.S8. Pulse annealing test results for individual grains from sample UH-LRB. In each cycle, the single-grain discs were given a regenerative dose of 93 Gy, and then annealed to a temperature of T °C. The remnant OSL signals for individual grains were then measured using a green laser stimulation at 125°C for 1.8 s, and at the end of each cycle a blue diode stimulation at 260 °C for 40 s was performed to remove all the signals. This measurement cycle was repeated several times with the annealing temperature T increased from 200 to 400 °C, with an increment of 20 °C. The sensitivity change in each cycle was corrected using the OSL signal of a test dose (measured after a cutheat of 200 °C). (a) Pulse annealing curves for four representative grains with different fast ratios. Grains with lower fast ratios (< 5) show a greater depletion in OSL towards higher annealing temperatures, indicating lower thermal stability; (b) Thermal remanent ratios (Fan et al., 2011) for 67 grains plotted as a function of their fast ratios. The thermal remanent ratio is calculated as the ratio of the remnant OSL signal measured after heating to 260 °C to that measured after heating to 200 °C. The results in Fig.S8b show that for a majority of grains with FR > 5, the reduction in OSL signal is small or negligible after a heating to 260 °C; in contrast, for most of grains with FR < 5, a heating to 260 °C has significantly depleted the OSL signal, suggesting grains with lower FR have lower thermal stability. This observation is most likely to attribute to a higher contribution of the unstable non-fast components to grains with low FR.

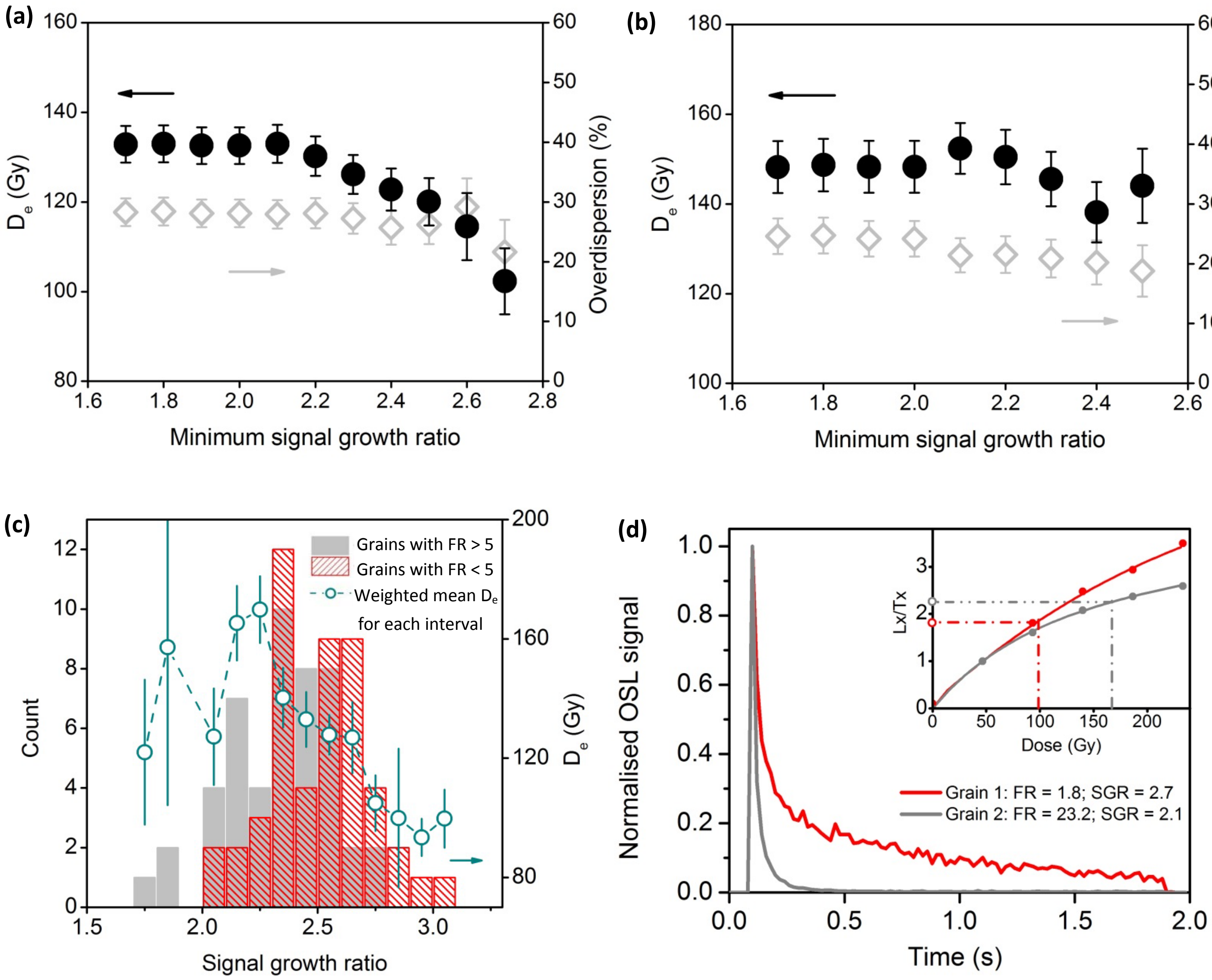

Fig.S9. (a) CAM D_es (filled circles) and overdispersion (open diamonds) of sample UH-LRB against the signal growth ratio (SGR) rejection threshold, for all grains passing the standard rejection criteria. The CAM D_e shows a decreasing tendency with increasing SGR threshold (i.e. shows a decreasing tendency with the dose saturation level increasing); (b) CAM D_es (filled circles) and overdispersion (open diamonds) of UH-LRB against the SGR rejection threshold, for grains passing the standard rejection criteria *and* with fast ratio (FR) > 5. In contrast to (a), for grains with FR > 5, there is no clear dependence of the CAM D_e on the SGR (i.e. no dependence of the CAM D_e on the dose saturation level); (c) Histograms showing the SGR distributions for 97 quartz grains of UH-LRB. The grey bars represent grains with FR > 5 and the hatches represent grains with FR < 5. The open circles represent the weighted mean D_es corresponding to each SGR interval (based on all grains without FR selection). The figure shows that grains with FR > 5 have a lower mean SGR (i.e. lower mean dose saturation level) compared to grains with FR < 5. Some grains with low FR, high dose saturation levels (high SGR, e.g. SGR > 2.5) and low D_e are identified. These grains likely to contain more non-fast components, therefore can yield underestimated D_es due to low thermal stability (see Figs. S7 and S8). These grains can also lead to a decrease of the CAM D_e with the SGR threshold increasing (as in Fig.S9a). Application of a FR rejection criterion (using a FR threshold value of 5) can reject these grains, thus eliminate the dependence of D_e on the dose saturation level (as in Fig.S9b); (d) Normalised OSL decay curves of two typical quartz grains of UH-LRB and their dose response curves (the inset): Grain 1—a grain which exhibits a low FR, a higher dose saturation level and a lower D_e value; and Grain 2—a grain which exhibits a high FR, a lower dose saturation level and a higher D_e value.

References

Aitken, M.J., 1985. Thermoluminescence Dating. Academic Press, London.

Bailey, R.M., 2000. The interpretation of quartz optically stimulated luminescence equivalent dose versus time plots. Radiation Measurements 32, 129–140.

Bowler, J.M., Johnston, H., Olley, J.M., et al., 2003. New ages for human occupation and climatic change at Lake Mungo, Australia. Nature 421, 837–840.

Fan, A.C., Li, S.H., Li, B., 2011. Observation of unstable fast component in OSL of quartz. Radiation Measurements 46, 21–28.

Guérin, G., Mercier, N., Adamiec, G., 2011. Dose rate conversion factors: update. Ancient TL 29 (1), 5–8.

Guérin, G., Mercier, N., Nathan, R., et al., 2012. On the use of the infinite matrix assumption and associated concepts: A critical review. Radiation Measurements 47, 778–785.

Guralnik, B., Li, B., Jain, M., Chen, R., Paris, R.B., Murray, A.S., Li, S.-H., Pagonis, V., Valla, P.G., Herman, F., 2015. Radiation-induced growth and isothermal decay of infrared-stimulated luminescence from feldspar. Radiation Measurements 81, 224–231.

Li, B., Li, S.-H., 2006. Comparison of De estimates using the fast component and the medium component of quartz OSL. Radiation Measurements 41, 125–136.

Nathan, R.P., Mauz, B., 2008. On the dose-rate estimate of carbonate-rich sediments for trapped charge dating. Radiation Measurements 43, 14–25.

Prescott, J.R., Hutton, J.T., 1994. Cosmic ray contributions to dose rates for luminescence and ESR dating: Large depths and long-term time variations. Radiation Measurements 23, 497–500.

Roberts, R.G., Galbraith, R.F., Yoshida, H., Laslett, G.M., Olley, J.M., 2000. Distinguishing dose populations in sediment mixtures: a test of single-grain optical dating procedures using mixtures of laboratory-dosed quartz. Radiation Measurements 32, 459–465.

Steffen, D., Preusser, F., Schlunegger, F., 2009. OSL quartz age underestimation due to unstable signal components. Quaternary Geochronology 4, 353–362.